

Extreme precipitation events over southern India during the year 2015- Curious interactions of El Nino, MJO, and associated waves

Rakesh Teja Konduru¹ and Mrudula G²

¹Department of Geography, Tokyo Metropolitan University, Tokyo, Japan

²Centre for Electromagnetics (CEM), Council of Scientific and Industrial Research (CSIR), National Aerospace Laboratories (NAL), Kodihalli, Bengaluru, India

November 22, 2022

Abstract

The cause of extreme precipitation events, which deadly flooded Tamil Nadu state of southern India during the northeast monsoon season of 2015 was investigated, and the results were presented in this paper. Though a strong El Nino prevailed during the events, the effect of El Nino is suppressed by the tropical variabilities in the Indian Ocean. A power spectrum analysis was performed to find out the kind of tropical variabilities in NCEP variables like wind fields, Omega, precipitation rate, and soil moisture at 0-10 cm. The spectrum analysis resulted in significant periodicities of 30-40 days and 7-20 days during the extreme events over southern India. Those frequencies were linked with the convectively coupled equatorial waves (CCEWs) like Madden-Julian Oscillations (MJO), and, it was found that the cause of El Nino's suppression is a manifestation of the CCEWs. The dynamical mechanism behind those interactions was investigated to know the specific connections of two major tropical variabilities El Nino and MJO. Further exploration was done by performing composite analysis of extreme precipitation events during historical El Nino (moderate to very strong) and MJO (active phases over the Indian Ocean) events from 1997-2014 to know the possible interaction between El Nino and MJO. The composite analysis contributed an insight into the interactions of El Nino and MJO. This analysis concludes a hypothesis, which states that if a prevailing, moderate to very strong El Nino as a background low-frequency wave superimposed with high-frequency wave like active MJO in the equatorial Indian Ocean during October-December season, then blended El Nino & MJO wave suppresses the effect of background prevalent El Nino. Such a clampdown of El Nino by blended El Nino & MJO wave roots the cause of extreme precipitation over the southeastern India. This study reveals a new dimension to the El Nino and MJO interactions in intraseasonal time scale, which could be exploited in the prediction of extreme precipitation events during northeast monsoon season.

1 **Extreme precipitation events over southern India during the year 2015-**

2 **Curious interactions of El Nino, MJO, and associated waves.**

3
4 Rakesh Teja Konduru^{1,2} and Mrudula G¹

5 *¹Department of Geography, Tokyo Metropolitan University, Tokyo, Japan.*

6 *²Centre for Electromagnetics (CEM), Council of Scientific and Industrial Research (CSIR), National*

7 *Aerospace Laboratories (NAL), Kodihalli, Bengaluru, India - 560017.*

8
9
10 **Submitted to**

11
12
13
14
15
16
17
18 Corresponding author email:- rakeshtejak@gmail.com

19

20

21

22

23

24 **Abstract**

25 The cause of extreme precipitation events, which deadly flooded Tamil Nadu state of
26 southern India during the northeast monsoon season of 2015 was investigated, and the results
27 were presented in this paper. Though a strong El Nino prevailed during the events, the effect of
28 El Nino is suppressed by the tropical variabilities in the Indian Ocean. A power spectrum
29 analysis was performed to find out the kind of tropical variabilities in NCEP variables like wind
30 fields, Omega, precipitation rate, and soil moisture at 0-10 cm. The spectrum analysis resulted in
31 significant periodicities of 30-40 days and 7-20 days during the extreme events over southern
32 India. Those frequencies were linked with the convectively coupled equatorial waves (CCEWs)
33 like Madden-Julian Oscillations (MJO), and, it was found that the cause of El Nino's suppression
34 is a manifestation of the CCEWs. The dynamical mechanism behind those interactions was
35 investigated to know the specific connections of two major tropical variabilities El Nino and
36 MJO. Further exploration was done by performing composite analysis of extreme precipitation
37 events during historical El Nino (moderate to very strong) and MJO (active phases over the
38 Indian Ocean) events from 1997-2014 to know the possible interaction between El Nino and
39 MJO. The composite analysis contributed an insight into the interactions of El Nino and MJO.
40 This analysis concludes a hypothesis, which states that if a prevailing, moderate to very strong El
41 Nino as a background low-frequency wave superimposed with high-frequency wave like active
42 MJO in the equatorial Indian Ocean during October-December season, then blended El Nino &
43 MJO wave suppresses the effect of background prevalent El Nino. Such a clampdown of El Nino
44 by blended El Nino & MJO wave roots the cause of extreme precipitation over the southeastern
45 India. This study reveals a new dimension to the El Nino and MJO interactions in intraseasonal

46 time scale, which could be exploited in the prediction of extreme precipitation events during
47 northeast monsoon season.

48

49 **Keywords**

50 El Nino, Madden-Julian Oscillations, Northeast Monsoon, convectively coupled equatorial
51 waves, Extreme precipitation, subtropical westerlies, and subtropical highs.

52 **1. Introduction**

53 Northeast monsoon (hereafter NEM; October-December, OND; it is also known as
54 retreating monsoon or winter monsoon; Dhar et al., 1983; Zubair, 2002) season is the main
55 cultivation season of states like Tamil Nadu, southern Andhra Pradesh in the South India and
56 also of Sri Lanka. In this season, all India receives 11 % of annual rainfall, and South India
57 receives up to 30%-60% of the annual precipitation. Apart from the Indian region, the Sri
58 Lankan region also receives up to 50% of annual rainfall. Also, the southeastern India receives
59 the maximum amount of rainfall during the same season and rain decreases further inland.
60 Rajeevan et al. (2012) studied the variability of the OND seasonal rains, and they found it to be
61 25 %, which is more than Indian summer monsoon rainfall variability (10%). Therefore, it is
62 crucial in predicting the NEM precipitation variability. Yadav R. K. (2011) had shown the
63 substantial variability of NEM rainfall in recent years. The extreme precipitation events in 2015
64 exemplify one such variability in NEM rainfall over the eastern coast of Tamil Nadu state in
65 India. Those extreme precipitation events occurred during three different periods, i.e. November
66 9 to 10, November 15 to 16 and November 30 to December 2 (hereafter these events are referred
67 as case-1, case-2, and case-3 respectively). These extreme events resulted in severe flooding,
68 consumed numerous deaths, and loss of properties in southeastern India, especially, the Chennai
69 that is totally inundated in floods. The World Meteorological Organization (WMO), India
70 Meteorological Department (IMD), and Regional Integrated Multi-Hazard Early Warning
71 System for Africa and Asia (RIMES) released their predictions in October 2015 that the strong
72 El Nino conditions might affect the NEM rainfall. However, their predictions could not clearly
73 address the potential impact region over southern India and Sri Lanka, and, they also stated that
74 the cause of such extreme events during NEM of southern India has been unresolved, and the

75 exact root of its origin requires proper investigation. The current paper investigates the ultimate
76 cause of those extreme events.

77 ***1.1 Background***

78 The fundamental variability of NEM rainfall is linked to ocean-atmosphere coupled
79 phenomenon like El Nino/Southern Oscillation (ENSO; Ropelewski and Halpert, 1987, 1989).
80 Most of the earlier studies had pointed out the linkage as inter-annual variability of NEM rainfall
81 with El Nino/Southern Oscillation (propagates in the background of the global weather as a low-
82 frequency wave); and their relationship supplemented by the presence of strong easterlies at 850
83 mb over the equatorial Indian Ocean and low-level moisture convergence. Suppiah (1997) has
84 studied the relationship between ENSO and NEM by compositing the extreme rainfall events and
85 found positive anomalies of NEM rainfall over southern India during El Nino years. Recent
86 studies showed that the relationship between ENSO and NEM had been strengthening over
87 South Asia (Zubin et al., 2006; Pankaj Kumar et al., 2007). Yadav R. K. (2011) has studied the
88 decadal relationship between ENSO and Inter-annual variability (IAV) of NEM rainfall. They
89 quoted that in El Nino years, NEM rainfall is either normal or above normal, which is also
90 shown by Rajeevan et al. (2012).

91 Few studies depicted the intra-seasonal variability (ISV) of NEM rainfall. Nageswara
92 Rao G. (1999) has reviewed the intra-seasonal relationship of NEM rainfall with Southern
93 Oscillation (SO) over South India, which explained the occurrence of peak rainfall over the same
94 region. Apart from it, northward propagation of organized convection and the presence of 20-60
95 day oscillation in NEM (Charlotte B. V. et al., 2012) are some of the features of ISV. Another
96 major global intra-seasonal pattern, which affects NEM rainfall is the Madden-Julian Oscillation

97 (MJO; Madden et al., 1971; Zhang, 2005). The MJO is one of the important tropical variability
98 associated with organized convection. Jia X et al. (2011), has shown the influence of MJO on the
99 northward transport of the moisture from the Indian Ocean and the Bay of Bengal during NEM.
100 Apart from above ISV of NEM rainfall, other tropical variabilities like equatorial waves that
101 propagate along the equator at different time scales (Wheeler et al., 1999). Those waves called as
102 convectively coupled equatorial waves (CCEW). Some of the identified CCEW are Kelvin
103 waves, equatorial Rossby waves, mixed Rossby & Gravity waves and Madden-Julian
104 Oscillation. The active phase of MJO especially is an enhanced zone of convection with co-
105 existence of CCEWs like equatorial trapped Kelvin waves and equatorial Rossby waves (Majda
106 et al., 2004; Mapes et al., 2006). In general, Kelvin waves are the most prominent source for
107 synoptic scale tropical rainfall variability, which travel through MJO (B Wang, 2002). There
108 have been very fewer studies done related to the impact of individual CCEWs, and CCEWs co-
109 existence with MJO on NEM rainfall. However, the interactions of MJO & Kelvin waves and
110 interactions of MJO & equatorial waves are well documented in individual works of Roundy,
111 2007; Hendon et al., 1994; Guo et al., 2014. Furthermore, those interactions are fundamentally
112 perceived in the experiment Year of Tropical Convection (YOTC; Gottschalck et al., 2010).

113 It is necessary to fill the gap of knowledge on the influence of individual CCEWs, and
114 blended CCEWs with MJO, on NEM rainfall. Apart from the El Nino & MJO interactions, its
115 impact on NEM is also imperative because they are the dominant modes of tropical variabilities.
116 Hendon et al. (2007) have observed the seasonal dependence of El Nino and MJO over the
117 equatorial Pacific Ocean. Current study outlines the interactions of El Nino and MJO, and, its
118 exact role in triggering the extreme events in 2015 over southeastern India during winter
119 monsoon.

120 2. Data and methodology

121 2.1 Observational and reanalysis data

122 The datasets employed in the analysis are 1) Tropical Rainfall Measuring Mission
123 (TRMM) 3B42 real time (RT) v7 0.25° precipitation rate (mm/day). TRMM 3B42 RT is a
124 combination of TRMM 3B40RT high-quality precipitation estimate (different satellites like
125 TRMM calibrated TMI, AMSR-E, SSM/I, AMSU, and MHS) and 3B41RT variable rain rate
126 infrared precipitation estimate from geostationary infrared observations. 2) Daily merged multi-
127 satellite-gauge real-time rainfall (mm/day) 0.25° resolution dataset for Indian region is
128 considered (Mitra et al., 2003, 2009, and 2013b). In this rainfall product, Global Precipitation
129 Measurement (GPM; Hou et al., 2014) project multi-satellite rainfall estimates are merged with
130 the IMD gauge data over Indian region. Satya Prakash et al. (2015) has studied accurateness in
131 the detection of heavy rain events by using TRMM and GPM rainfall datasets, which became our
132 motive to show the three extreme precipitation events by using that space-borne rainfall
133 observation. 3) Global Precipitation Climatology Product (GPCP) v1.2 1.0° daily precipitation
134 rate (mm/day) is also utilized (Huffman et al., 2001). 4) India Meteorological Department (IMD)
135 0.5° daily rainfall (mm/day) is acquired to select the moderate to heavy rain events over Indian
136 region (Mitra et al., 2009). Moreover, 5) National Center for Environmental Research Prediction
137 - National Center for Atmospheric Research (NCEP-NCAR) reanalysis-1, (Kalnay et al., 1996) 6
138 hourly 2.5° data set is obtained to analyze the dynamic atmosphere conditions during the events.
139 From the NCEP reanalysis, variables like wind fields, Omega, relative humidity up to 17
140 pressure levels, and surface variables like sea level pressure, soil moisture at 0-10 cm, and lifted
141 index were chosen. Apart from above variables, precipitation rate of NCEP-NCAR reanalysis-1
142 in a Gaussian grid of T64 is also exploited in the analysis.

143 *2.2 Methodology*

144 Anomalies of selected variables from NCEP-NCAR reanalysis-1 dataset were calculated
145 for the period 1981-2015 based on the 1981-2010 climatology. A composite of the 2015 winter
146 monsoon extreme precipitation cases were created by using anomalies over the region $10^{\circ}\text{S} -$
147 $40^{\circ}\text{N} \ \& \ 40^{\circ}\text{E} - 120^{\circ}\text{E}$ (it covers entire Indian region and neighboring oceans; that region was
148 named as domain-1). The power spectrum analyses of the composites of each case were
149 performed to know the dominant modes of periodicities during NEM over the area $8^{\circ}\text{N}-20^{\circ}\text{N} \ \& \$
150 $75^{\circ}\text{E}-85^{\circ}\text{E}$ (the region was named as domain-2). Domain-2 cover only land fractions of
151 southern India, which was also named as NEM region because winter monsoon rainfall is
152 received in most of the parts of that region. From the composites, mean was removed, detrended,
153 and tapered before passing through Fast Fourier Transform (FFT). These preprocessing steps
154 minimize the chances of ringing and leakage. Subsequently, those periodicities were employed to
155 extract convectively coupled equatorial waves over $5^{\circ}\text{S} - 5^{\circ}\text{N}$ (CCEWs) by using a band-pass
156 filter for each wave separately over each grid point. Some of the CCEWs like Kelvin waves were
157 obtained from band-pass filtering of the variables for wavenumber 1 to 14 as done by Wheeler et
158 al. (1999) and Straub et al. (2002). The equatorial Rossby waves were filtered in a similar
159 manner, but for wavenumber -10 to -1 as quoted by Kiladis et al. (2009). All of the variables
160 were initially detrended and then tapered in time and filtering was done with a specific
161 wavenumber of the individual CCEWs by using discrete Fourier transform on the periodic data.
162 The MJO wave was extracted by applying a band-pass filter for wavenumbers 1 to 5 as
163 mentioned in Wheeler et al. (1999) over a time window 30-90 days.

164 Another composite analysis of historical extreme rainfall events from 1981-2014 and
165 1997-2014 (table-1) was carried out over southern India during OND season. The rain events

166 were clustered based on the criteria used by Pattanaik et al. (2010) and Guhathakurta et al.
167 (2011) into heavy and extreme rainfall events if daily rainfall is more than 64.5 mm in domain-2.
168 The extreme rain events were separated prudently into El Nino and Normal events (Normal
169 events do not include El Nino and La Nina year events) by using the Oceanic Nino Index (ONI).
170 The ONI is defined as three months running mean of sea surface temperature anomalies in the
171 region Nino 3.4 (5°S- 5°N & 120°W-170°W). The El Nino is further classified as moderate if
172 ONI is 1.0 to 1.4, strong El Nino if ONI is 1.5 to 1.9) and very strong El Nino if ONI is more
173 than or equal to 2.0. Those El Nino and Normal extreme rainfall events were further categorized
174 into active MJO (active phases 2 and 3 of MJO) and weak MJO events over the Indian Ocean
175 region by using Real-time Multivariate MJO RMM1 and RMM2 index. The Real-time
176 Multivariate MJO Index is obtained by projecting daily anomalies of 850 mb zonal wind, 200 mb
177 zonal wind, and outgoing longwave radiation onto the multiple-variable EOFs (Wheeler et al.,
178 2004). The MJO was considered strong if the index magnitude is more than one. Otherwise, it is
179 hard to discern weak MJO signal in the considered meteorological variables. Thus, categorized
180 extreme rainfall events were grouped into different composites like Normal, El Nino, MJO, and
181 El Nino & MJO. Further, the difference among those composites was calculated and analyzed to
182 understand the interactions of El Nino & MJO, El Nino & Normal, Normal & MJO, El Nino &
183 MJO with MJO, and El Nino & MJO with El Nino during extreme events in OND season. The
184 differences of composites were validated with the Student's t-test, which ensures the robustness
185 of residuals, and to see whether the composite states significantly differs from the base state; and
186 only more than 95 % significant part was showed in the difference composites.

187 **3. Results and Discussions**

188 During OND season of 2015, the southeastern India witnessed extreme rainfall events
189 during three different periods, i.e. November 9 to 10 (case-1), November 15 to 16 (case-2) and
190 November 30 to December 2 (case-3), which caused flooding in the southeastern parts of Tamil
191 Nadu state in India.

192 *3.1 Synoptic Observations*

193 Composites of GPM and TRMM rainfall were created in case-1, case-2, and case-3. The
194 rainfall is widespread over southeastern India in both case-1 (fig 1 a1) and case-2 (fig 1 b1),
195 whereas, in case-3 (fig 1 c1) rainfall is localized in nature over Chennai. All of these events lead
196 to heavy floods in Chennai and its neighborhoods, which will be the region of focus in the
197 current section. In case-1 (fig 1 a2), the negative anomalies of sea level pressure over southern
198 India represent the formation of a low-pressure area (LPA) in the south Bay of Bengal (hereafter
199 BOB). Subsequently, it strengthened to a deep depression in the south BOB and moved
200 northwestward over to land after crossing the southeastern coast at Pondicherry. Similarly, case-
201 2 (fig 1 b2) is an LPA with cyclonic circulation laid at 1000 mb, in southern BOB. At the same
202 time, to the south of LPA below the equator, two cyclonic circulations are noticed at 1000 mb
203 and 850 mb. However, an upper air cyclonic circulation (UAC) is observed in case-3 (fig 1 c2)
204 over southeastern India. The noteworthy point is that the source of moisture to all of these cases
205 is southerlies from the equatorial Indian Ocean (shown in the lower panel of figure 1). However,
206 the sinks of moisture are different kinds of mesoscale convective systems formed near the
207 southeastern coast of India.

208 Figure 2 demonstrates the time series of a vertical cross-section of meteorological
209 variables averaged over 12°N-13°N & 80°E over Chennai and its neighborhoods. Very strong

210 updrafts (fig 2c, Omega) from surface to 200 mb, with strong positive relative humidity
211 anomalies from 850 mb to 500 mb (fig 2e), sufficient negative lifted index anomalies (fig 2b, red
212 line), and adequate fall in sea level pressure (fig 2b, green line) helped the mesoscale convective
213 system in case-1 to develop further from low pressure area to deep depression. The presence of
214 very less wind shear (fig 2d) supported the deep depression to sustain without being dispersed
215 and resulted with a peak precipitation of ~70 mm/day (fig 2a). However, in case-2, the weather
216 conditions are similar to case-1 but low in magnitude, resulted in the development of mesoscale
217 convective system related to well-marked low. Along with those weather conditions, the lifted
218 index (fig 2b) maintained the meteorological instability to support the cyclonic circulation by
219 moisture convergence and resulted in peak precipitation of 50 mm/day (fig 2a). Interestingly, in
220 Case-3, though there was an enormous amount of relative humidity (fig 2e), it did not contribute
221 much rain due to weak updrafts (fig 2c) and high wind shear (fig 2d). Therefore, case-3 event did
222 not show much rainfall as compared to case-1 & case-2, but the rainfall received is around 30
223 mm/day (fig 2a). The rainfall in case-1 clearly represents extreme precipitation event and in
224 case-2 & case-3 as rather heavy rain events based on the criteria used by Pattanaik et al. (2010),
225 and Guhathakurta et al. (2011).

226 *3.2 NCEP anomalies and overview of wind fields*

227 Composites of NCEP zonal wind anomalies were created for three cases. In case-1,
228 cyclonic circulation associated with a deep depression formed at 1000 mb (fig 1a) laid over
229 southern India extends up to 500 mb (fig 3d left column). A positive velocity potential at 850 mb
230 over South India and BOB represents the presence of converging winds (fig 3g; green color
231 contour). At 500 mb positive velocity potential (fig 3d) seems to shift eastward, and a zone of
232 negative velocity potential appears over the western coast of southern India. However, the

233 cyclonic circulation at 200 mb vanishes due to diverging winds represented by negative velocity
234 potential (fig 3a; magenta color contour). While in case-2, over southern India, cyclonic
235 circulation extends from 1000 to 500 mb (fig 3e), and a positive velocity potential shows the
236 presence of converging winds at these levels. The cyclonic circulation at 200 mb disappears due
237 to diverging winds (fig 3b), which is demonstrated by negative velocity potential. Nevertheless,
238 in case-3, UAC is weak in nature at 850 mb (fig 3i), but it is strong at 500 mb (fig 3f) that covers
239 entire southern India and represented by positive velocity potential at those levels. The presence
240 of diverging winds represented by negative velocity potential at 200 mb (fig 3c) terminates the
241 circulation at this level. The similarity in these three cases is the presence of westerlies that
242 dominated over the North Indian Ocean around 80°E at 850 mb & 500 mb, but these westerlies
243 are found to be weak in case-1.

244 The motivating point is that all of the three cases have shown southerly wind anomalies
245 at 850 mb (fig 4g-h-i) and 500 mb (fig 4d-e-f). In case-2 and case-3, southerly wind anomalies
246 are strong as compared to case-1. The presence of an active zone of positive relative humidity
247 anomalies (green color contour) over southern India and southerly winds clearly portrays the
248 manner by which these winds bring moisture from the Indian Ocean (source) and moves further
249 north through southern India. Consequently, the mesoscale convective systems developed over
250 south India act as a sink of moisture and southerly winds serve as a carrier for it. In general,
251 during NEM over southern India, northeasterly winds prevail (Dhar et al., 1983), and they act as
252 a carrier of moisture from the source BOB. However, these three cases are different in
253 concerning both the origin and transport of moisture over southern India.

254 *3.3 Vertical cross-sections of dynamical parameters*

255 Figure 5 shows the longitudinal and latitudinal vertical cross-sections of Omega and
256 relative humidity anomalies. The figure 5a & 5b represents mean of OND season of 2015 and
257 figure 5c & 5d shows mean for the period November 8 to 16, 2015, which consists of case-1 &
258 case-2 events. These two events are observed to be similar regarding meteorological conditions
259 as explained in previous sections. The left, and right panels in figure 5 describe Omega
260 anomalies scaled by zonal wind anomalies and meridional wind anomalies respectively.
261 Moreover, the shaded portion in the figure 5a & 5c illustrates relative humidity anomalies
262 averaged over 5°S–5°N. The presence of strong positive relative humidity anomalies and strong
263 updrafts over the Pacific Ocean conveys about the shift in the Walker circulation to the east (fig
264 5a), which in general happens during climatic variability like El Nino as explained by Philander
265 (1990). Besides, over maritime continent subsidence of dry air is clearly observed. An interesting
266 feature of strong updrafts until 600 mb is perceived over 80°E with sufficient positive anomalies
267 of relative humidity. Figure 5c is a mean of variables as mentioned above from November 8 to
268 16 (which includes extreme and rather heavy rain events of OND season 2015). It is similar to
269 the fig 5a, except very strong updrafts over the Pacific Ocean and around 80°E in the Indian
270 Ocean. The presence of strong updrafts and substantially high relative humidity until 500 mb
271 level supports the anomalous convergence of moisture.

272 Figure 5b & 5d shows vertical cross-sections along latitude 40°S–40°N averaged over
273 75°E–85°E. The updrafts over equator are weak as seen in figure 5b. However, updrafts over
274 30°N and 30°S are seen from lower troposphere to upper troposphere and at mid-troposphere
275 respectively. Over 10°N–15°N, subsidence of dry air is witnessed. The figure 5d is a mean from
276 November 8 to 17, 2015, in which stout updrafts and very high moisture are seen until 500 mb
277 around 10°N–15°N. As a result, these anomalous circulations of moisture affect the southern part

278 of India that comes in 10°N-15°N. In addition to it, significant moisture convergence is observed
279 around 30°S & 30°N. These latitudinal and longitudinal cross-sections exhibit strong updrafts
280 due to convergence and transport of moisture around 80°E from the north Indian Ocean to 10°N -
281 15°N & 75°E–85°E region of India.

282 These results imply the solid connections between sink & source regions of wind fields
283 and humidity to the large-scale tropical variabilities. Unfortunately, there was no such direct link
284 found with tropical variabilities like El Nino. In general, during El Nino, the source of moisture
285 is same as observed in current cases, but the carrier is easterlies over Northern Indian Ocean.
286 These easterly winds are not seen during the current events. Moreover, no such profitable link
287 observed between NEMR with IOD due to neutral Indian Ocean Dipole (IOD) conditions during
288 2015 NEM because only during positive IOD phase southerlies and the Indian Ocean acts as a
289 carrier and source of moisture respectively. Thus, the source and carrier of moisture created a
290 curiosity to know about the exact linkage of moisture transport during the current cases with the
291 kind of tropical variability.

292 **3.4 The dominant periodicities of ISV over NEM region.**

293 Power spectrum analysis is performed over nine meteorological parameters. These
294 parameters include, precipitation rate (both TRMM 3B42 and NCEP reanalysis), mid-
295 tropospheric temperature (MTT; 500 mb), mid-tropospheric humidity (MTH; 500 mb), zonal
296 wind at 925 mb & 200 mb, meridional wind at 925 mb & 200 mb, and soil moisture at 0-10 cm
297 (fig 6). Accordingly, dominant periodicities of these parameters are obtained over NEM region
298 (8°N - 20°N & 75°E - 85°E; OND). The analysis suggests that few of the parameters like upper
299 tropospheric humidity (fig 6d), Zonal wind at 200 mb (fig 6f) and soil moisture at 0-10 cm (fig

300 6i) showed periodicities of 30-40 days with 90% significance, whereas Zonal wind at 200 mb
301 displayed similar variability with 80% significance. The soil moisture is analyzed to diagnose
302 whether a built-in memory of soil moisture, which is about weeks to two months or much longer
303 than that of atmospheric variables (Vinnikov et al., 1991; 1996; Entin et al., 2000), plays any role
304 in retaining the periodicity of the tropical variability. Encouragingly, soil moisture spectrum very
305 clearly exhibits the ability of it to store the 30-40 days oscillation. Also, MTH also exhibited 30-
306 40 variability in the tropical atmosphere (e.g., Mote et al., 2000; Tian et al., 2006). Whereas, the
307 30-40 day periodicity is barely significant in MTT (fig 6c), zonal wind 925 mb (fig 6e), and
308 precipitation rate (fig 6a & 6b; TRMM & NCEP). Moreover, 7-20 day periodicity is also
309 observed with 90 % significance in almost all parameters. This analysis brings out an idea of the
310 presence of 30-40 days and 7-20 oscillation during OND of 2015.

311 The presence of 7-20 days oscillation in the power spectrum analysis, along with that the
312 features suchlike anomalous westerlies near to the equator in three extreme event cases at 850
313 mb (fig 3) resemble them like Kelvin wave as described by Thomson, W. (1989). The twin
314 cyclonic circulations across the equator over the southern Indian Ocean in case-1 & case-2
315 corresponds to equatorial Rossby waves with 9-72 day oscillation as described by G. N. Kiladis
316 et al. (1996) respectively. These notable waves propagate to the east and west respectively. On
317 the other hand, at 850 mb the meridional wind anomalies show (fig 4) northward propagation
318 during case-2 & case-3. That signifies the observed westerly anomalies near to the equator are
319 not only Kelvin waves by its own, but accompanied by a particular kind of oscillations like
320 Madden-Julian Oscillations (30-90 days; MJO). These observations show that the extreme
321 rainfall events could be due to MJO, equatorial Rossby waves, and Kelvin waves, which are also
322 known as convective coupled equatorial waves (CCEWs).

323

324 ***3.5 Convectively Coupled Equatorial Waves (CCEW)***

325 NCEP anomalies of the wind field, velocity potential, sea level pressure, and
326 precipitation rate anomalies are employed to extract the corresponding CCEW for the events as
327 described in section 2.2. The above meteorological variables were passed through 30-90 days
328 band-pass filter, which filtered out only those unusual patterns that have the same period as of
329 the MJO (fig 7; In this section only filtered variables were analyzed). It is evident that in most of
330 the cases, westerly wind anomalies are dominated near to the equator, and two cyclonic
331 circulations appear across the equator at 850 mb, which is associated with the MJO (Wheeler et
332 al., 1999). In case-1, the well-marked negative anomalies of sea level pressure (magenta color
333 dashed line at 1000 mb) over southern India are associated with cyclonic circulation formed due
334 to the deep depression at 1000 mb (fig 7d). Apparently, that could be a region of the enhanced
335 organized convection of MJO over southern India, which is indicated by positive velocity
336 potential (green color contour). The convectively coupled enhanced convective region of the
337 MJO could be identified as Kelvin wave, which is reported in the works of Nakazawa (1988),
338 Takayabu et al. (1991), Dunkerton et al. (1995), and Straub et al. (2002). These Kelvin waves
339 propagate eastward as reflected from the high westerly wind anomalies at 850 mb in the Indian
340 Ocean. At higher levels like 200 mb, filtered negative velocity potential anomaly (blue dash line)
341 depicts diverging wind fields with easterly zonal wind anomalies (fig 7a).

342 However, in case-2, the presence of negative sea level pressure anomalies to both sides of
343 the equator beckoned it as an equatorial Rossby wave which propagates westwards (fig 7e). This
344 observation is in agreement with the results obtained by Kiladis et al. (1995), Wheeler et al.

345 (2000), and Roundy et al. (2004b). A very active zone of westerly wind anomalies shifted to
346 northwards around 80°E demonstrating the presence of Kelvin wave, which is a major
347 component of MJO for enhanced convection that propagates eastward. Together with above
348 CCEWs, interestingly, in case-2, all of the dominant modes of equatorial variability are observed
349 at the same region. This co-existence of CCEWs could be attributed to the substantial
350 enhancement of the westerly winds over the same area, which is evident from the wind field
351 observations in the figure 7e. This kind of co-existence of dominant modes of CCEWs like MJO,
352 Kelvin wave, and equatorial Rossby wave immensely contributed to the mesoscale convective
353 systems development over the southern India. The similar results related to the co-existence of
354 CCEWs are also observed in the work of Roundy et al. (2010). The co-existence of CCEWs
355 around 80° E could prolong the convective activities over the same region. Such a prolonged
356 convective activity due to the co-existence of CCEWs is also reported by Roundy (2007). In
357 case-3, negative sea level pressure anomalies over the Indian Ocean (at surface magenta color
358 dashed line) correspond to the synoptic system developed over that region, which is represented
359 by a positive velocity potential (fig 7f). However, the twin cyclonic circulations across the
360 equator in 850 mb zonal wind anomaly show the presence of equatorial Rossby waves. The
361 westerly wind anomalies at 850 mb are close to the equator and are not as strong as seen in case-
362 2. One of the peculiar features of case-3 is the existence of anomalous trough in westerlies at 200
363 mb (fig 7c), which are not regarded in case-1 and case-2 that are dominated by subtropical highs.
364 This anomalous trough in westerlies separates the case-3 from remaining cases upper
365 tropospheric zonal wind anomalies. It clearly implies that along with MJO some other
366 phenomenon might have existed during case-3, which modulated the subtropical westerlies to
367 form a low trough and pushed the lower level westerlies towards the equator.

368 The striking point is that the enhanced convection of the MJO has contributed to the case-
369 1, case-2, and case-3 rainfall events with different convectively active modes. Figure 8 illustrates
370 the filtered convectively active modes of CCEWs. Figure 8a shows the MJO, and equatorial
371 Rossby waves in filtered 850 mb, 200 mb zonal winds, and precipitation rate, which supported in
372 the formation of a tropical depression over the southern Indian Ocean that caused extreme rain
373 over southeastern India in case-1. A similar kind of CCEWs existed in case-3, which influenced
374 the mesoscale convective system over southeastern India (fig 8c). However, case-2 is a
375 combination of different kinds of CCEW like Kelvin waves and equatorial Rossby waves within
376 MJO and contributed to widespread rain over southeastern India (fig 8b). This analysis confirms
377 the influence of CCEWs on different mesoscale convective systems, which caused extreme
378 events over southeastern India.

379 Another crucial thing is that though CCEWs has affected the weather over southeastern
380 India, its strong influence even in the presence of very strong El Nino in the background is
381 uncommon. Since 2015 is reported as a year of very strong El Nino, it is not apparent to have
382 such a kind of dominated westerlies near the equator, which could suppress the impact of
383 easterlies associated with El Nino lower tropospheric levels over the Indian Ocean region.
384 Generally, in the past, during very strong El Nino years of 1982 & 1997 in OND season, all of
385 the extreme rainfall events are accompanied with easterly wind anomalies at 850 mb, and there
386 were no traces of suppression of easterly winds associated with El Nino by westerly winds
387 associated with the MJO. Therefore, it is crucial to know the interactions between MJO and El
388 Nino, and the mechanism of it, which caused extreme precipitation events. For this analysis,
389 case-2 event is selected out of three cases to explore the interaction between the MJO and El

390 Nino because in case-2, Kelvin and equatorial Rossby waves co-existed within MJO, and it is
391 assumed as an ideal condition.

392

393 ***3.6 Interactions between El Nino and MJO***

394 The extreme events (precipitation more than 64.5 mm/day) from 1997-2014 were
395 composited as Normal, MJO, El Nino, and El Nino & MJO (hereafter these composites are
396 called as NC, MC, EC, and EMC respectively) during OND season. Here, EMC events were
397 those cases in which El Nino and MJO exist together. These composites were assumed as waves
398 and interactions among those composites were investigated. Here, Normal composite wave does
399 not to include El Nino, La Nina and active MJO events of phase 2 & 3. The list of extreme
400 rainfall events used in the composites was presented in table-1, and the procedure for selecting
401 composites was already discussed in section 2.2. These composites were prepared (table-2) by
402 using NCEP zonal winds (850 mb, 200 mb), and precipitation rate anomalies (NCEP and GPCP;
403 TRMM was not considered because it does not include 1997 very intense El Nino).

404 Figure 9 illustrates a difference between the different combinations of composite waves
405 (it is called as the residual), like, EC & NC, EC & MC, EMC & NC, EMC & MC, MC & NC,
406 and EMC & EC, which are denoted as A, B, C, D, E and F residuals respectively. These
407 residuals exemplify all of those remnant waves, which are dominant during the past extreme
408 events in OND season. Persuasive results are noticed from residuals in the zonal wind anomalies
409 (upper panels in figure 9) and precipitation rate (GPCP; lower panel in figure 9). Though zonal
410 wind anomalies are similar in the residuals A, B, C and D at 850 mb (fig 9 a3-d3), the
411 precipitation rate anomalies are positive only in C and D (fig 9 c4-d4) over southeastern coast of

412 India, northern Sri Lanka, the southwestern part of the BOB, and over the Indian Ocean.
413 However, negative anomalies of precipitation rate persist in the residuals A and B (fig 9 a4-b4)
414 over the same regions. This kind of dissimilarity in precipitation rate even in the presence of
415 similar kind of anomalous wind fields is questionable. To get contrasts among the composites A,
416 B, C, and D it is important to have an appropriate understanding of the each residual. As
417 mentioned earlier, the A residual is a difference between EC and NC waves. The presence of
418 anomalous easterlies at 850 mb in (fig 9 a3) exhibits the dominating nature of EC wave over the
419 NC wave. As a result, dryness due to less precipitation is witnessed over the Indian Ocean and
420 southeastern India (fig 9 a4). A similar situation persists in the residual B, which is a difference
421 between EC and MC wave, where a leftover wave of El Nino dominates. As a result,
422 southwestern peninsular India, and northern Sri Lanka show significant positive anomalies of
423 rainfall (fig 9 b4). Likewise, easterlies at 850 mb are stronger in B (fig 9 b3) residual than in A,
424 which conveys the importance of leftover El Nino wave and its domination over the MC wave.
425 The C residual is the remnant of blended wave EMC with Normal wave, and, D residual is the
426 balance of EMC wave with MC wave. In C residual, EMC wave dominates in the foreground,
427 whereas, in D residual El Nino wave controls the foreground. In both of these residuals, strong
428 easterlies dominate at 850 mb over the Indian Ocean (fig 9 c3 and fig 9 d3), which might cause
429 wetness over the southeastern coast of India, southwestern BOB, and the Indian Ocean regions
430 (fig 9 c4 and fig 9 d4).

431 In addition to easterlies at lower tropospheric levels in residuals A, B, C and D, the upper
432 tropospheric wind fields like subtropical westerlies (STW) at 200 mb (fig 9 a1-d1) and 500 mb
433 levels (fig 9 a2-d2) could have moderately influenced the weather of southern India. These
434 residuals showed very clear cyclonic circulations in STW. Due to relatively strong nature of

435 STW's, its influence extended equatorward up to South India. This deepening of trough related
436 to STW triggered the transport of moisture from the south BOB to northwards, which might be
437 another reason for positive precipitation anomalies over South India in C and D residuals. These
438 striking aspects of STW are in agreement with the results obtained by Li C et al. (2015).
439 Moreover, the strength of STW is more in D composite (fig 9d1) than in any other composites,
440 which clearly implies the remnant El Nino wave is relatively strong in D residual than in any
441 other residuals.

442 An interesting situation attains with residual F, in which the remnant of EMC blended
443 wave and EC wave is MJO wave. The remnant MJO wave is appreciably seen over the equator
444 around 80°E as strong westerly anomalies at 850 mb (fig 9 f3) and strong easterlies at 200 mb
445 (fig 9 f1). In the F residual, whole central India is quietly dry, whereas, southeastern India (Tamil
446 Nadu coast, and Andhra Pradesh coast) and North Sri Lanka shows a significant positive
447 anomaly of precipitation rate of the order 1-2 mm/day (fig 9 f4). The extraordinary amount of
448 precipitation over the coast of southeastern India can be essentially attributed to the residual
449 wave F, which propagates over the background El Nino low-frequency wave, and MC wave.
450 Also, over the Indian Ocean, significant positive anomalous precipitation is observed in F
451 residual. It implies that the blended EMC wave interacts with the background EC wave to cause
452 anomalous precipitation over the regions mentioned above. Consequently, this kind of the
453 distinctive features of EMC blended wave and EC wave interactions was noticed during the
454 extreme events of 2015 OND season, which caused extreme precipitation over the southeastern
455 India. The residual E also shows a pattern which is similar to that of F residual, but westerly
456 wind strength at 850 mb and 500 mb is too weak (fig 9 e3 & 9 e2). The strength of upper
457 tropospheric easterlies at 200 mb (fig 9 e1) is feeble, and southern India appears to be dry due to

458 lack of precipitation (fig 9 e4). Nevertheless, a significant amount of precipitation is observed
459 over the Indian Ocean in E residual. Moreover, the upper tropospheric strong easterlies weaken
460 the subtropical westerlies (STW) in both E and F residuals (fig 9 e1 & 9 f1). The weakening of
461 STW in these residuals is attributed to the anticyclonic circulations, which could be another
462 reason for dryness over northern and central India in the residuals E and F. Thus; these residuals
463 are necessary in the case of blended EMC waves over a region.

464 **3.7 The vertical cross-section of zonal and meridional circulations in the residuals.**

465 The vertical cross-section of the longitudinal variations of relative humidity and omega
466 (weighted by zonal winds) from 20°E to 280°E averaged over latitude 5°S to 5°N are illustrated
467 for A, B, C, D, E, and F residuals in figure 10, which depicts the different branches of the
468 Walker circulation. These various branches of Walker circulation over the equator is
469 demonstrated by Bjerknes (1969) and Walker et al. (1932). The subsidence of dry and stable air
470 over the central Pacific Ocean is observed in residuals E (fig 10e) and F (fig 10f), whereas rising
471 limb of moist air is witnessed over the same region in the residuals A, B, C and D (figure 10a to
472 10d respectively). The above-mentioned zonal circulation in residual E is associated with the
473 normal Walker Circulation with rising branch over maritime continent and descending branch
474 over central and the eastern Pacific Ocean, but the same circulation in residuals A, B, C, and D
475 are affected by atmospheric variability mainly El Nino. Due to the effect of El Nino, the rising
476 branches of moist air in residuals A, B, C, and D over the Indian Ocean are weakened except
477 over the East African coast, which is the case of Walker Circulation variability due to El Nino as
478 explained by Philander (1990). Furthermore, subsidence of dry air over the maritime continent
479 and ascending moist air over the Indian Ocean is perceived in the residuals E and F. However, in
480 the residuals A, B, C, and D rising limb of moist air exists over the western Indian Ocean and

481 subsidence of dry wind over the maritime continent and the eastern Indian Ocean. Besides, the
482 ascending moist wind is recognized over the Indian Ocean in residuals E and F. Exceptionally in
483 residual F; the rising branch is healthy around 80°E. Consequently, the ascending limb at 80°E in
484 residual F well matches with the ascending limb over the Indian Ocean during November 8 to
485 17, 2015 as shown in figure 5c. Hence, anomalous Walker circulation branch could account the
486 significant positive rainfall anomalies over southern India, which is in agreement with the studies
487 of Allan et al. (1986).

488 Similarly, a latitudinal variation of relative humidity and Omega from 30°S to 30°N
489 averaged over 75°E to 85°E is shown in figure 11. It displays the meridional overturning Hadley
490 circulation (HC; Held et al., 1980) variations among the residuals. The residuals of E (fig 11e)
491 and F (fig 11f) shows the standard Hadley circulation with rising branch over the equator and
492 subsidence over the subtropics around 30°S & 30°N. However, the residuals of A, B, C, and D
493 (fig 11a to 11d) shows ascending moist air over the equator with less meridional extent, and a
494 strong rising of moist air is noticed around 30°S & 30°N. The sturdy ascent over subtropics is
495 associated with the impact of El Nino, which strengthened the STW as explained before; these
496 observations over subtropics are in agreement with the studies of Seager et al. (2003).
497 Interestingly, in the residuals of E and F, rising moist air is identified over the tropics around
498 10°N to 15°N and is much stronger in F residual. Therefore, a healthy ascent of moist air in
499 residual F matches with the ascent over the Indian Ocean during November 8 to 17 in 2015.
500 Strikingly, these results elicit the large-scale variability of the atmosphere in both meridional and
501 zonal circulations, which appreciably affected the local weather of southern India with the
502 transport of moist air.

503 **3.8 The response of precipitation to residual waves.**

504 The current section focuses on the response of precipitation over southeastern India to the
505 zonal winds in the residual waves. Figure 12 summarizes the precipitation rate (averaged over
506 8°N - 16°N & 75°E - 85°E) responds to the zonal wind anomalies (averaged over the regions 0° - 6°N
507 & 70°E - 80°E for MJO wave and 2°S - 4°N & 90°E - 98°E for El Nino wave) of composites NC,
508 MC, EC, and EMC. The motive behind in selecting different regions for MJO and El Nino is to
509 showcase the domination of westerly wind anomalies in residuals E and F for MJO region, and
510 easterly wind anomalies in A, B, C, and D residuals for El Nino region. A linear relationship
511 was constructed between zonal wind anomalies and precipitation rate of each composite. In the
512 case of NC composite, the response of precipitation to the change in zonal wind anomalies is
513 steady, which is apparent from the noticeable correlation coefficient of 0.086. Whereas, MC
514 composite precipitation response to the zonal wind anomalies seems to fluctuate with a
515 reasonable standard deviation of 3.32 and a moderate correlation of 0.26. Notably, on some
516 occasions, strong westerlies over the region for MJO showed high precipitation response over
517 southeastern India, but when individual events are examined, the response of precipitation over
518 the same region is weak, which makes MC composite quite trivial. Interestingly, in EC
519 composite, the zonal wind anomalies and precipitation rate is considerably positively correlated
520 with a correlation of 0.97 and sensible standard deviation of 1.26, with dominated easterlies. As
521 a result, precipitation responds appreciably positive to the strength of easterlies, which markedly
522 causes more wetness over the southeastern India. However, there are some events of easterlies,
523 with weak precipitation response and sometimes dryness over the southeastern India.

524 In the blended EMC wave, the response of precipitation rate anomalies to the zonal wind
525 anomalies exhibited dual nature with a correlation coefficient of 0.05. In the dual nature of EMC
526 wave, the precipitation response of dominated EC wave is high as compared to the dominated

527 MC wave. In the past, very few such EMC wave cases are noticed during OND season. An
528 interesting situation was achieved, wherein, residuals C, D, and F showed the strong response of
529 precipitation to the easterly wind anomalies in C, D, and westerly wind anomalies in F. As a
530 result, F residual significantly suppresses the easterlies of EC wave, and gives rise to the MC
531 wave from EMC blended wave to dominate in the foreground. Consequently, precipitation
532 responds substantially to the westerly zonal wind anomalies, which causes rain over the
533 southeastern India. The other residuals do not respond like F residual, but they too are necessary
534 for additional interactions among composite waves, and their corresponding precipitation
535 response. Remarkably, residual D with prevailing easterlies responds with high rainfall over the
536 southeastern India like in F, but in the case of remaining residuals precipitation decreases over
537 the same region. With the background of composite wave and residual wave interactions, their
538 precipitation responses, leads to a hypothesis. The hypothesis states that ‘beforehand, if there is
539 a prevailing moderate to very strong El Nino in the background as a low-frequency wave (EC),
540 and, if another high-frequency wave like MJO propagates over the background (MC) in the
541 equatorial Indian Ocean during October – December season, then the blended wave EMC
542 interacts with prevalent EC wave. This interaction creates a remnant wave MJO, which
543 dominates in the foreground of EC wave. This remnant MJO wave considerably suppresses the
544 effect of background EC wave by weakening easterlies at 850 mb and replacing it with very
545 strong westerlies around 80° E near to equator like in F residual. Eventually, remnant MJO wave,
546 in turn, affects the weather of southeastern India with the development of mesoscale convective
547 systems, which contributes extreme precipitation as a positive response over the same region and
548 neighboring regions’. Such a unique behavior and make-up of F residual are not accompanied
549 with any other residuals. As a result, the residual F is unique in nature, and such cases are

550 infrequent in the past. Similar analysis is performed quantitatively by stretching the analysis
551 period to 1981-2014 (here, NCEP precipitation rate is used instead of GPCP because GPCP data
552 set is available only until 1997) so that another strong El Nino case is included in the study and
553 the number of samples of data would be more. This quantitative analysis also accomplishes
554 similar results as seen in the previous qualitative study with GPCP observations. Therefore, these
555 two types of analysis demonstrate the robustness of the hypothesis. It clearly indicates the
556 domination of blended wave EMC over background state El Nino wave. Therefore, blended El
557 Nino & MJO wave has shown two different kinds of convolutions. Firstly, mixed wave
558 dominates the foreground MJO wave in residual E, and secondly, mixed wave dominates
559 background El Nino wave in F residual. As a result, the domination of mixed wave over El Nino
560 and MJO states requires special attention.

561

562

563

564

565

566

567

568

569

570 4. Summary

571 In this work, extreme precipitation events during the northeast monsoon season of 2015
572 were analyzed. Extreme rainfall associated with case-1 is connected to the deep tropical
573 depression formed over the northern Indian Ocean. The case -2 event is related to the LPA, and
574 case-3 rain event is due to the UAC over southern India. This analysis also ignited an outlook
575 that tropical variability could influence the wind fields, which can alter the carrier of moisture in
576 OND season from northeasterly winds to southerly winds.

577 The power spectrum analysis of meteorological variables during winter monsoon of 2015
578 over NEM region revealed the significant dominant periodicities of 30-40 days in some of the
579 variables like mid-tropospheric humidity, zonal wind at 200 mb and soil moisture. Likewise,
580 another important periodicity of 2-17 days was seen with most of the variables. Subsequently,
581 these dominant periodicities are filtered for MJO (30-90 days), Kelvin and equatorial Rossby
582 waves in the anomalies in the zonal wind at 850 mb and 200 mb, precipitation rate, sea level
583 pressure and velocity potential. These filtered atmospheric variables illuminated the dominant
584 mode of tropical variability as MJO and associated CCEWs, which influenced the weather over
585 southern India by enhanced convection. Though MJO appeared weak during the extreme events,
586 its remnants interacted with the background atmosphere. One of the important observations is,
587 though El Nino is very strong propagating in the background atmosphere in 2015 during OND
588 season, its influence is suppressed over the Indian Ocean by remnants of MJO & associated
589 CCEWs with very vigorous westerly winds. This kind of interaction is uncommon in the past
590 episodes of El Nino; as a result, the interaction of El Nino and remnants of MJO & associated
591 CCEWs during winter monsoon of 2015 engraved its identity in the literature.

592 Further, a composite analysis of past extreme precipitation events of moderate to strong
593 El Nino events, active MJO events, and Normal events from 1997-2014 in OND season is
594 exploited to study the interactions of El Nino wave with El Nino & MJO blended wave (F
595 residual). This kind of interaction resulted in a hypothesis that, if El Nino prevailing as
596 background low-frequency wave, superimposed with high-frequency MJO over the Indian Ocean
597 during OND season, then blended El Nino & MJO wave could suppress the easterlies of El Nino
598 wave by replacing with westerlies, which are remnants of MJO, in turn causes extreme
599 precipitation over the southern India. The influence of residuals on vertical cross-sections of
600 relative humidity and Omega revealed an anomalous branch of the Walker circulation over the
601 Indian Ocean in F residual of El Nino & MJO and El Nino composite wave, which nourished the
602 moisture to the mesoscale convective systems formed over southern India. Similarly, latitudinal
603 variations showed an anomalous meridional circulation over the southern India around 10° N to
604 15° N, which also fed moisture to the mesoscale convective systems over the region mentioned
605 above. Also, the meridional flow of humidity to the western edge of subtropical anticyclones,
606 transport moisture from the equatorial Indian Ocean to subtropics, which is revealed from the
607 analysis of F residual (obtained from historical extreme events analysis) and also found in case-
608 1, case-2, and case-3 events. This transport of moisture could feed the mesoscale convective
609 systems over southern India. As a result, current investigation very clearly depicts the
610 importance of the residual F during mesoscale convective systems over the southeastern Indian
611 region in intra-seasonal scale. Fruitfully, it explains the kind of tropical variability, occasional
612 interactions between El Nino & MJO, and large-scale phenomenon behind the extreme events
613 over southern India. The co-existence of MJO and El Nino is a general phenomenon seen over
614 tropical regions, but the interactions in which MJO masks out the effects of El Nino is crucial.

615 The evidence related to such suppression of El Nino by MJO is very slim in literature. Sensitivity
616 studies could be helpful in the supplementary understanding of the interaction between El Nino
617 & MJO. Such studies will be essential in the prediction of extreme events associated with those
618 different interactions of El Nino and MJO. A systematic, detailed study of interactions of El
619 Nino and other CCEW like Kelvin wave and equatorial Rossby wave, during winter monsoon,
620 would be investigated in future, which will fill gaps in the tropical variability study of NEM over
621 the Southern Indian region. Lastly, this year's unique interaction between a well-developed,
622 strong El Nino and MJO wave is a textbook example of the scientific society, and it began in the
623 Indian Ocean and caused extreme precipitation events over southeastern India.

624

625

626

627

628

629

630

631

632

633

634 **Acknowledgements**

635 This work is a part of the INCOMPASS project 2015-2018 supported by Ministry of
636 Earth Sciences (MoES). Both of the authors are obliged to the Director CSRI National
637 Aerospace Laboratories (CSIR-NAL) and Head Centre for Electromagnetics Department (CEM)
638 Bangalore India, for providing facilities and support. The lead author Mr. Rakesh Teja Konduru
639 is grateful to MoES for providing research fellowship in the INCOMPASS project. The authors
640 also thankful to co-researcher for their help in preparing research draft.

641

642

643

644

645

646

647

648

649

650

651

652

653 **References**

- 654 Bjerknes, J., 1969. Atmospheric teleconnections from the equatorial Pacific. *Mon. Weather Rev.*
655 *Vol 97, 3,163-172.*
- 656 Dhar, O. N., Rakhecha P. R., 1983. Forecasting northeast monsoon rainfall over Tamil Nadu,
657 India. *Mon. Weather Rev.* 111, 109-112.
- 658 Dunkerton, T. J., Crum, F. X., 1995. Eastward propagating 2-15 day equatorial convection and
659 its relation to the tropical intraseasonal oscillations. *J. Geophys. Res.* 100, 25781-25790.
- 660 Entin, J. K., Robock, A., Vinnikov, K. Y., Hollinger, S. E., Liu, S., Namkhai, A., 2000.
661 Temporal and spatial scales of observed soil moisture variations in extratropics. *J.*
662 *Geophys. Res.* 105, 11865-11877.
- 663 Gottschalck, J., Wheeler, M., Weickmann, K., Vitart, F., Savage, N., Lin, H., Hendon, H.,
664 Waliser, D., Sperber, K., Nakagawa, M., Prestrelo, C., Flatau, M., Higgins, W., 2010. A
665 Framework for Assessing Operational Madden-Julian oscillation forecasts: A CLIVAR
666 MJO working group project. *Bull. Amer. Meteor. Soc.* 91,9, 1247-1258.
- 667 Guhathakurta, P., Sreejith, O. P., Menon, P. A., 2011. Impact of climate change on extreme
668 rainfall events and flood risk in India. *J. Earth Sys. Sci.* 120(3), 359-73.
- 669 Guo, Y., Jiang, X., Waliser, D. E., 2014. A Systematic Relationship between the Representations
670 of Convectively Coupled Equatorial Wave Activity and the Madden-Julian Oscillation in
671 the Climate Model Simulations. *J. Clim.* 28, 1881-1904.
- 672 Held, I. M., Hou, A. Y., 1980. Nonlinear axially symmetric circulations in a nearly inviscid
673 atmosphere. *J. Atmos. Res.* 37, 515-533.

- 674 Hendon, H. H., Wheeler M. C., Zhang C., 2007. Seasonal dependence of the MJO-ENSO
675 relationship. *J. Clim.* 20, 531-543.
- 676 Hou, A. Y., Kakkar, R. K., Neeck, S., Azarbarzin, A. A., Kummerow, C. D., Kojima, M., Oki,
677 R., Nakamura, K., Iguchi, T., 2014. The global precipitation measurement mission. *Bull.*
678 *Am. Meteor. Soc.* 95, 701-22.
- 679 Huffman, Adler G. J. R. F., Morrissey, M. M., Curtis, S., Joyce, R., McGavock, B., Susskind, J.,
680 2001. Global precipitation at one-degree daily resolution from multi-satellite
681 observations. *J. Hydrometeorology*, 2, 36-50.
- 682 Jia, X., Chen, L. J., Ren, F. M., Li, C. Y., 2011. Impacts of the MJO on winter rainfall and
683 circulation in China. *Adv. Atmos. Sci.* 28(3), 521-533, doi:10.1007/s00376-010-9118-z.
- 684 Kalnay, E., Kanamitsu, M., Kistler, R., Collins, W., Deaven, D., Gandin, L., Iredell, M., Saha,
685 S., White, G., Woollen, J., Zhu, Y., Leetmaa, A., Reynolds, R., Chelliah, M., Ebisuzaki,
686 W., Higgins, W., Janowiak, J., Mo, K. C., Ropelewski, C., Wang, J., Roy Jenne, Dennis
687 Joseph, 1996. The NCEP/NCAR 40-year reanalysis project. *Bull. Amer. Meteor. Soc.* 77,
688 437-470.
- 689 Kiladis, G. N., Wheeler, M., 1995. Horizontal and vertical structure of observed tropospheric
690 equatorial Rossby waves. *J. Geophys. Res.* 100(D11), 22981-22997.
- 691 Kiladis, G. N., Wheeler, M. C., Haertel, P. T., Straub, K. H., Roundy, P. E., 2009. Convectively
692 coupled equatorial waves. *Rev. Geophys.* 47.
- 693 LI, C., Sun, J. L., 2015. Role of the subtropical westerly jet waveguide in a southern China
694 heavy precipitation in December 2013. *Adv. Atmos. Sci.* 32(5), 601-612.

- 695 Liebmann, B., Hendon, H. H., Glick, J. D., 1994. The relationship between the tropical cyclones
696 of western Pacific and the Indian Ocean and Madden-Julian Oscillation. *J. Meteor.Soc.*
697 *Japan*, 72 401-412.
- 698 Madden, R. A., Julian, P. R., 1971. Detection of a 40-50 day Oscillation in the Zonal Wind in the
699 Tropical Pacific. *J. Atmos. Sci.* 28, 702-708.
- 700 Majda, A. J., Khouider, B., Kiladis, G. N., Straub, K. H., Shefter, M. G., 2004. A model for
701 convectively coupled tropical waves: Nonlinearity, rotations and comparison with
702 observations. *J. Atmos. Sci.* 61, 2188-2205.
- 703 Mapes, B., Tulich, S., Lin, J., Zuidema, P., 2006. The mesoscale convective life cycle: building
704 block or prototype for large-scale tropical waves? *Dyn. Atmos. Oceans*, 42, 3-29.
- 705 Mitra, A. K., Dasgupta, M., Singh, S. V., Krishnamurti, T. N., 2003. Daily rainfall for Indian
706 monsoon region from merged satellite and rain gauge values. *J. Hydrometeorology*, 4(5),
707 769-781.
- 708 Mitra, A. K., Bohra A. K., Rajeevan M. N., and Krishnamurti T. N., 2009: Daily Indian
709 precipitation analysis from a merge of rain-gauge data with the TRMM/TMPA satellite-
710 derived rainfall estimates. *J. Meteorol. Soc. Jap.*, Vol. 87A, 265-279.
- 711 Mitra, A. K., Mornin, I. M., Rajagopal, E. N., Basu, S., Rajeevan, M. N., Krishnamurti, T. N.,
712 2013b. Gridded daily Indian monsoon rainfall for 14 seasons: Merged TRMM and IMD
713 gauge analyzed values. *J. Earth Sys. Sci.* 122(5), 1173-1182.
- 714 Nageswara Rao, G. 1999. Variations of the SO Relationship with Summer and Winter Monsoon
715 Rainfall over India: 1872-1993. *J. Clim.* 12, 3486-3495.

- 716 Nakawaza, T., 1988. Tropical superclusters within intraseasonal variations over the western
717 pacific. *J. Meteor. Soc. Japan*, 66, 823-839.
- 718 Pankaj, Kumar, Rupa Kumar, K., Rajeevan, M., Sahai, A. K., 2007. On the recent strengthening
719 of the relationship between ENSO and northeast monsoon rainfall over South Asia. *Clim.*
720 *Dyn.* 8, 649-660.
- 721 Pattanaik, D. R., Rajeevan, M., 2010. Variability of extreme rainfall events over India during
722 southwest monsoon season. *Meteorol. Appl.* 17, 88-104.
- 723 Philander, S. G., 1990. *El Nino, La Nina, and the Southern Oscillation*. 293 pp, Academic, New
724 York.
- 725 Rajeevan, M., Unnikrishnan, C. K., Jyoti Bhate, Niranjan Kumar, K., Sreekala, P. P., 2012.
726 Northeast monsoon over India: variability and prediction. *Meteorol. Appl.* 19, 226-236.
- 727 Ropelewski, C. F, Halpert, M. S., 1989. Precipitation pattern associated with the high index
728 phase of the Southern Oscillation. *J. Clim.* 2, 268-284.
- 729 Ropelewski, C. F., Halpert, M. S., 1987. Global and regional scale precipitation patterns
730 associated with the El Nino/Southern Oscillation. *Mon. Wea. Rev.* 115, 1606-1626.
- 731 Roundy, P. E., William Frank, M., 2004a. A climatology of waves in the Equatorial region. *J.*
732 *Atmos. Sci.* 61, 2105-2132
- 733 Roundy, P. E., William Frank, M. 2004b. Effects of low-frequency wave interactions on
734 intraseasonal oscillations. *J. Atmos. Sci.* 61: 3025-3040
- 735 Roundy, P. E., Kiladis, G. N., 2006. Observed relationship between oceanic Kelvin waves and
736 atmospheric forcing. *J. Clim.* 19, 5253-5272.

- 737 Roundy, P. E., 2008. Analysis of convectively coupled Kelvin waves in the Indian Ocean MJO.
738 J. Atmos. Sci. 65,4, 1342-1359
- 739 Satya Prakash, Mitra, A. K., Pai, D. S., Amir Agha Kouchak, 2015. From TRMM to GPM: How
740 well can heavy rainfall be detected from space? *Adva. Water Res.* 88, 1-7.
- 741 Seager, R., Harnik, N., Kushnir, Y., Robinson, W., Miller, J., 2003. Mechanisms of
742 hemispherically symmetric climate variability. *J. Clim.* 16, 2960-2978.
- 743 Straub, K. H., Kiladis, G. N., 2002. Observations of convectively coupled Kelvin wave in the
744 eastern Pacific ITCZ. *J. Atmos. Sci.* 59, 30-53.
- 745 Straub, K. H., George Kiladis, N. 2010. Observations of a Convectively Coupled Kelvin Wave in
746 the Eastern Pacific ITCZ. *J. Atmos. Sci.* 59, 30-53.
- 747 Suppiah, R., 1997. Extremes of Southern Oscillation phenomenon and the rainfall of Sri Lanka.
748 *Int. J. Climatol.* 17, 87-101.
- 749 Takayabu, Y. N., Murakami, M., 1991. The structure of super cloud clusters observed in 1-20
750 June 1986 and their relationship to easterly waves. *J. Meteor Soc. Japan*, 69, 105-125.
- 751 Vinnikov, K. Y., Yeserkepova, I. B., 1991. Soil moisture, empirical data and model results. *J.*
752 *Clim.* 4, 66-79.
- 753 Vinnikov, K. Y., Robock, A., Speranskaya, N. A., Schlosser, A., 1996. Scales of temporal and
754 spatial variability of midlatitude soil moisture. *J. Geophys. Res.* 101, 7163-7174.
- 755 Walker, G. T., Bliss, E., 1932. *World Weather. V. Mem. Roy. Met. Soc.* 4, 53-84.
- 756 Wang, B., 2002. Kelvin Waves., doi:10.1006/rwas.2002.0191.
- 757 Wheeler, M., Kiladis, G. N., 1999. Convectively coupled equatorial waves: Analysis of clouds

758 and temperature in the wavenumber-frequency domain. *J. Atmos. Sci.*, 56, 374-399.

759 Wheeler, M., Kiladis, G. N., Webster, P. J., 2000. Large-scale dynamical field associated with
760 the convectively coupled equatorial waves. *J. Atmos. Sci.* 57, 613-640

761 Wheeler, M. C., Hendon, H. H., 2004. An all-season real-time multivariate MJO index:
762 development of an Index for monitoring and prediction. *Mon. Wea. Rev.* 132, 1917-1932.

763 Zhang, C., 2005. Madden-Julian oscillation. *Rev. Geophys.* 43.

764 Zubair, L., Ropeleswski, C. F., 2006. The strengthening relationship between ENSO and
765 northeast monsoon rainfall over Sri Lanka and southern India. *J. Clim.* 19, 1567-1575.

766 Allan, R. J., Lindesay, J., Parker, D., 1996. *El Nino Southern Oscillation and Climatic
767 Variability.*, 402 pp., CSIRO, Collingwood, Victoria, Australia.

768 Climate Prediction Center (CPC) Oceanic Nino Index. 2006., Climate Prediction Center,
769 National Centers for Environmental Prediction, national Weather Service, U.S.
770 Department of Commerce, Maryland.

771 Consensus statement on the Forecast for the 2015 Northeast Monsoon Season (October –
772 December) Rainfall and Temperature over South Asia. First Session of Winter South
773 Asian Climate Outlook Forum (WinSASCOF-1). Chennai, India. October 15-17 2015.

774 The NCAR Command Language (Version 6.3.0) [Software]. 2016, Boulder, Colorado:
775 UCAR/NCAR/CISL/TDD. <http://dx.doi.org/10.5065/D6WD3XH5>.

776 Tropical Rainfall Measurement Mission Project (TRMM). 2011, TRMM/TMPA 3B42RT 3
777 Daily TRMM and Others Daily Rainfall Estimate V7. Goddard Space Flight Center
778 Distributed Active Archive Center (GSFC DAAC), Greenbelt, MD.

779 Table 1: Extreme rainfall events from 1981-2014 in OND were selected based on criteria if daily rainfall
 780 is more than 64.5 mm. The events from 2000-2014 are confirmed based on the India Meteorological
 781 Department weather reports. Here, yellow color represents extreme rain events related to El Nino & MJO.

S.No.	Years	Heavy rainfall events
1	1981	Oct 26-29
2	1982	Oct 17-21, Nov 2-6
3	1985	Nov 19-24, Dec 13-15
4	1986	Oct 3-6, Oct 29-Nov 3 , Oct 5-7
5	1987	Oct 16-17, Nov 3-5 , Nov 13-14, Dec 5-7
6	1989	Dec 2-4, Nov 11-14, Oct 7-9
7	1990	Oct 1-3, Oct 23-25 , Oct 29-Nov 4 , Nov 26-27
8	1991	Oct 28-Nov 1, Nov 13-18
9	1992	Oct 4-5 , Oct 9-11, Nov 14-19
10	1993	Oct 8-12, Oct 31-Nov 1, Nov 6-12 , Nov 24-25 , Dec 24-26
11	1996	Oct 1-5, Oct 9-15, Oct 17-21 , Nov 8-9, Nov 21-26 , Dec 7-16
12	1997	Oct 12-16, Oct 21-25, Oct 28-29, Nov 2-8, Nov 14-18 , Nov 26-27, Dec 3-8
13	1999	Oct 1-6 , Oct 14-15 , Nov 18-21, Nov 27-29 , Dec 21-22
14	2001	Oct 5-6, Oct 15-16, Nov 5-7 , Dec 21-22
15	2002	Oct 7-15, Oct 25-30 , Nov 5-10 , Dec 6

16	2003	Oct 19-21, Dec 15, Dec 24
17	2005	Oct 8-9 , Oct 10-15 , Oct 18-19, Oct 21-24, Nov 4-8, Nov 20-24, Dec 2-3, Dec 9-10
18	2008	Oct 13-16 , Oct 20-26, Nov 16-17, Nov 23-30, Dec 9-11
19	2009	Oct 1-4, Oct 29-30, Nov 3-9 , Nov 15-16, Dec 2-4, Dec 14-16
20	2012	Oct 1-3, Oct 6-7, Oct 13-15, Oct 19-22, Oct 31-Nov 4 , Dec 3-5
21	2013	Oct 20-26, Nov 2-4, Nov 16-18 , Nov 24-28, Dec 12-13
22	2014	Oct 9-13, Oct 17-19, Oct 26-27 , Nov 13-15, Nov 21-22 , Dec 29-30

782

783

784

785

786

787

788

789

790

791

792

793 Table 2: The composites of Normal, El Nino, MJO events and their combinations.

S.NO.	Composites	No. of Events
1	Normal	47
2	Normal & MJO	21
3	El Nino	17
4	El Nino & MJO	11
	Total	96

794

795

796

797

798

799

800

801

802

803

804 List of Figures

805 **Figure 1:** Top row in the panel is composite of GPM precipitation rate (mm/day) and below row in the
806 panel is TRMM 3B42RT precipitation rate during the three cases, i.e., case-1 (left-most column), case-2
807 (middle column), and case-3 (right most column). The dashed contour are NCEP sea level pressure
808 negative anomalies and solid contour are NCEP sea level pressure positive anomalies. Those Vectors
809 represent NCEP wind field anomalies.

810 **Figure 2:** These plots are drawn over latitude 12°N-13°N and longitude 80°E which covers Chennai
811 region of India from October 1 to December 31 of 2015. a) NCEP precipitation rate (mm/day) averaged
812 over the mentioned region. b) The red color solid line is NCEP lifted index and green color solid line are
813 NCEP sea level pressure, c) NCEP omega anomalies are, d) NCEP zonal wind anomalies, and e) NCEP
814 relative humidity anomalies. Note NCEP relative humidity is available up to 300 mb. All of these
815 variables were composited for case-1 (Nov 9-Nov 10), case-2 (Nov 15-Nov 16), and case-3 (Nov 30-Dec
816 2), which are mentioned as black color dashed vertical lines.

817 **Figure 3:** NCEP zonal wind anomalies composite is created for three cases i.e. (a-d-g) case-1 (Nov 9 to
818 10), b-e-h) case-2 (Nov 15 to 16), and c-f-i) case-3 (Nov 30-Dec 2). Each row of the panel represents a
819 pressure level, which is shown to the right of the last column of the panel. A lowermost row of the panel
820 corresponds to the zonal wind anomalies at 850 mb, and a topmost row of the panel represents 200 mb
821 zonal wind anomalies. Shaded portion is zonal wind anomalies and vectors are anomalous wind. The
822 solid contours are positive velocity potential anomalies, and dashed lines are negative velocity potential
823 anomalies contoured from - 6 to 6 with an interval of three.

824 **Figure 4:** The NCEP meridional wind (m/s) anomalies composite is created for three cases i.e. (a-d-g)
825 case-1 (Nov 9 to 10), b-e-h) case-2 (Nov 15 to 16), and c-f-i) case-3 (Nov 30-Dec 2). Each row of the
826 panel represents a pressure level, which is shown to the right of the last column of the panel. A lowermost
827 row of the panel corresponds to the meridional wind anomalies at 850 mb, and a topmost row of the panel

828 represents 200 mb meridional wind anomalies. Shaded portion is meridional wind anomalies and vectors
 829 are anomalous wind. The solid contours are positive relative humidity (%) anomalies contoured from -50
 830 to 50 with an interval of 15. Note NCEP Relative Humidity data is available only up to 300 mb pressure
 831 levels.

832 **Figure 5:** It demonstrates vertical cross-sections of omega, and relative humidity. Left column shows
 833 longitudinal cross-section (a, c) and right column (b, d) represents latitudinal cross-sections. Longitudinal
 834 cross-sections are averaged over 5°S-5°N, and latitudinal cross-sections are averaged over 75°E-85°E. Top
 835 row (a, b) represents OND anomalies, and bottom row shows (c, d) mean of the composite from
 836 November 8 to 17, 2015. Here vectors are omega values scaled w.r.t to zonal wind for longitudinal
 837 section and meridional for latitudinal section

838 **Figure 6:** Power spectrum is shown for a) TRMM 3B42 precipitation rate, b) NCEP precipitation rate, c)
 839 air temperature, d) zonal wind at 850 mb, e) soil moisture at 0-10 cm, and f) Omega at 850 mb, during
 840 October-December of 2015 over southern Indian region (8°N-20° N & 70°E-85°E) is calculated. Green
 841 Line shows Markov Red Noise spectrum; red line show upper 95% confidence bounds; and the blue line
 842 shows lower 5% bounds. The x-axis represents periodicity and y-axis represents variance.

843 **Figure 7:** It displays MJO band pass filtered NCEP zonal wind (m/s) anomalies composite is created for
 844 three cases i.e. (a-d-g) case-1 (Nov 9 to 10), b-e-h) case-2 (Nov 15 to 16), and c-f-i) case-3 (Nov 30-Dec
 845 2). Each row of the panel represents a pressure level, which is shown to the right of the last column of the
 846 panel. A lowermost row of the panel corresponds to the meridional wind anomalies at 850 mb, and a
 847 topmost row of the panel represents 200 mb meridional wind anomalies. Shaded portion and vectors are
 848 band-pass filtered (30-90 days) zonal wind anomalies. In the bottom panel, the dashed contours are
 849 negative sea level pressure (mb) anomalies and solid contours are positive sea level pressure anomalies
 850 contoured for -0.3, -0.1, and 0.3. In the first panel, the dashed contour is a negative velocity potential
 851 anomaly, and the solid line is positive velocity potential anomaly contoured for -4.0, -0.5, 0.5, and 4.0.

852 **Figure 8:** It display Hovmueller plots of band-pass filtered (30-90 days for MJO, 9-72 days for equatorial
 853 Rossby waves, and 2.5-17 days for Kelvin waves) a) zonal wind anomalies at 850 mb (m/s), b) zonal
 854 wind anomalies at 200 mb (m/s) and c) NCEP precipitation rate (mm/day), they are averaged over 10°S-
 855 10°N. Shaded portion represents MJO filtered waves. Whereas, blue color solid line and red color solid
 856 line represent Kelvin waves and equatorial Rossby waves respectively. Dotted black line points the dates
 857 during which case-1, case-2, and case-3 happened.

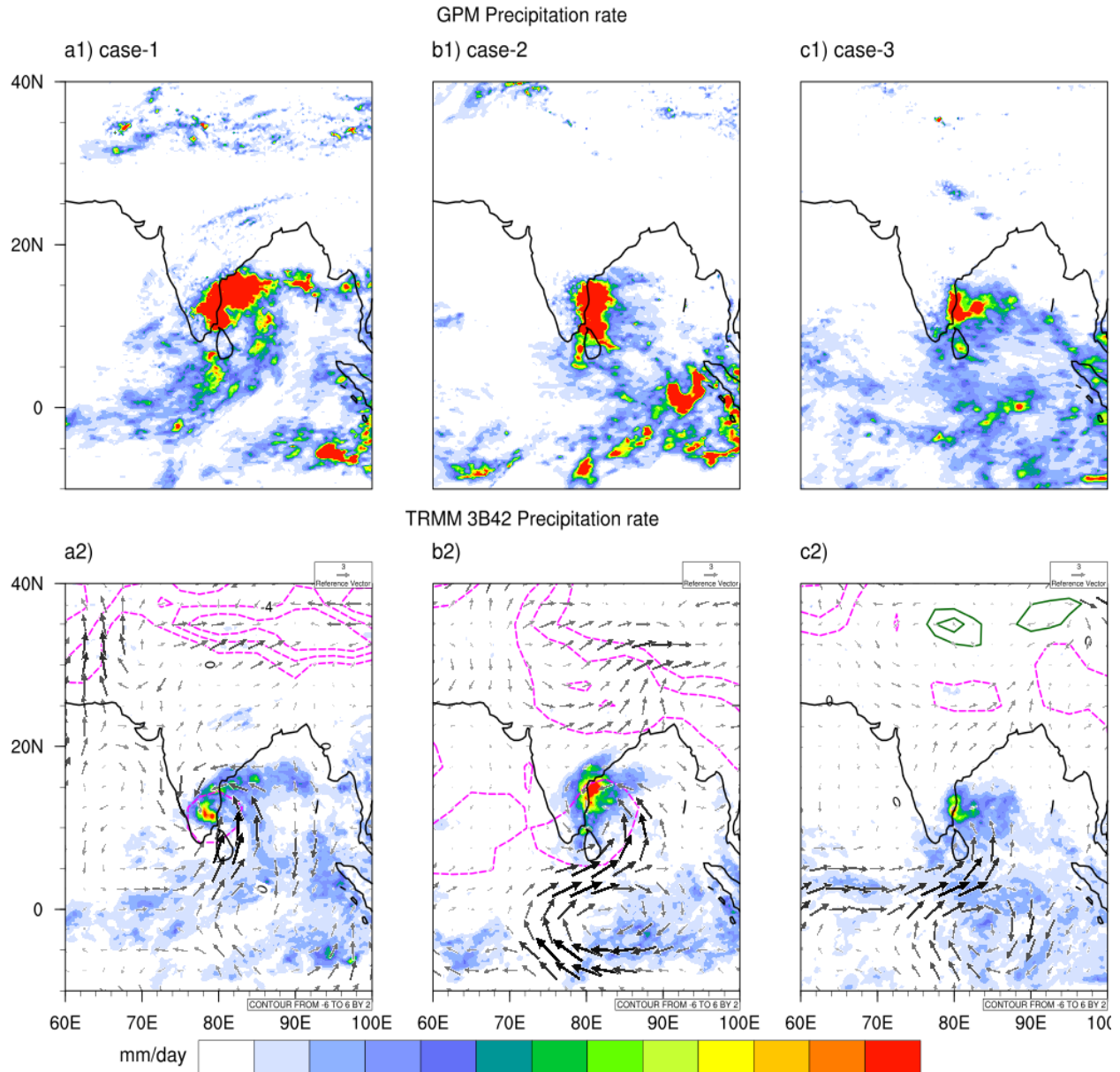
858 **Figure 9:** It summarizes the residuals, which are difference between (A) E and N composite (left
 859 column), (B) E and M composite, (C) EM blended and N composite, (D) EM blended and M composite,
 860 (E) M and N composite, and (F) EM blended and E composite; for NCEP zonal wind anomalies (m/s) and
 861 GPCP precipitation rate (mm/day) anomalies. Each row of the panel represents a pressure level, which is
 862 shown to the right of the last column of the panel. A lowermost row of the panel corresponds to the wind
 863 anomalies at 1000 mb, and precipitation rate anomalies and a topmost row of the panel represents 200 mb
 864 zonal wind anomalies. The shaded portions of a second bottom row of the panel to top most rows are
 865 zonal wind anomalies. In all of the plots only, more than 95 % significant values are shown (Student's t-
 866 test is performed at critical value 0.05).

867 **Figure 10:** It summarizes the zonal vertical cross-sections of omega, and relative humidity anomalies of
 868 A, B, C, D, E, and F residuals, which are differences of E & N, E & M, EM & N, EM & M, M & N and
 869 EM & E composites, and these composites are explicitly discussed in section 3.6. These longitudinal
 870 cross-sections were averaged over 5°S-5°N. Here vectors are omega values scaled w.r.t to the zonal wind,
 871 and colored region shows relative humidity anomalies.

872 **Figure 11:** It describes the meridional vertical cross-sections of omega, and relative humidity anomalies
 873 of A, B, C, D, E, and F residuals, which are differences of E & N, E & M, EM & N, EM & M, M & N,
 874 and EM & E composites, and these composites are explicitly discussed in section 3.6. These latitudinal

875 cross-sections are averaged over 75°E-85°E. Here vectors are omega values scaled w.r.t to the meridional
876 wind, and colored area shows relative humidity anomalies.

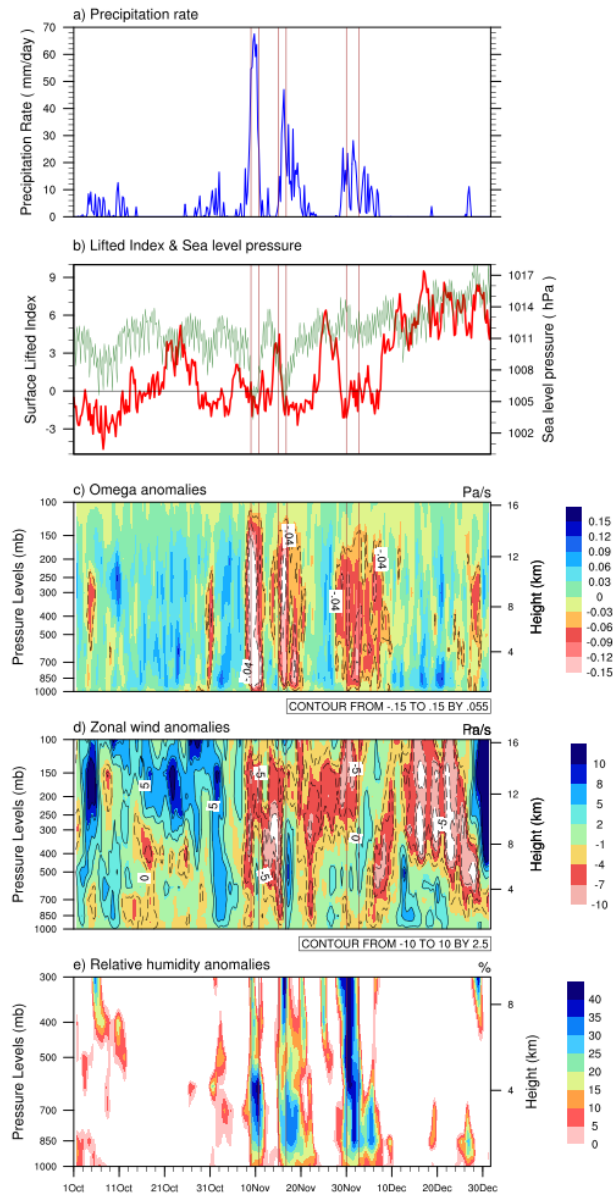
877 **Figure 12:** It demonstrates the response of GPCP precipitation anomalies to NCEP zonal wind anomalies
878 in MJO (red; M), Normal (green; N), El Nino (blue; E) and El Nino & MJO mixed wave (magenta; EM)
879 composites. Here composites are created for a period 1997-2014 in OND season. The black color markers
880 represent the residuals A, B, C, D, E, and F; these residuals are interactions of M & N, E & N, E & M,
881 EM & N, EM & M and EM & E composites respectively. The precipitation anomalies shown above are
882 area averaged over 8°N-16°N & 75°E-84°E, and zonal wind anomalies are area averaged over 0°-6°N &
883 70°E-80°E for MJO and 2°S-4°N & 90°E- 98°E for El Nino composites. The statistical characteristics like
884 p-value (p), correlation coefficient (r), and standard deviations (std) of each composite are also shown in
885 the figure.



886

887 **Figure 1:** Top row in the panel is composite of GPM precipitation rate (mm/day) and below row in the
 888 panel is TRMM 3B42RT precipitation rate during the three cases, i.e., case-1 (left-most column), case-2
 889 (middle column), and case-3 (right most column). The dashed contours are NCEP sea level pressure
 890 negative anomalies and solid contours are NCEP sea level pressure positive anomalies. Those Vectors
 891 represent NCEP wind field anomalies.

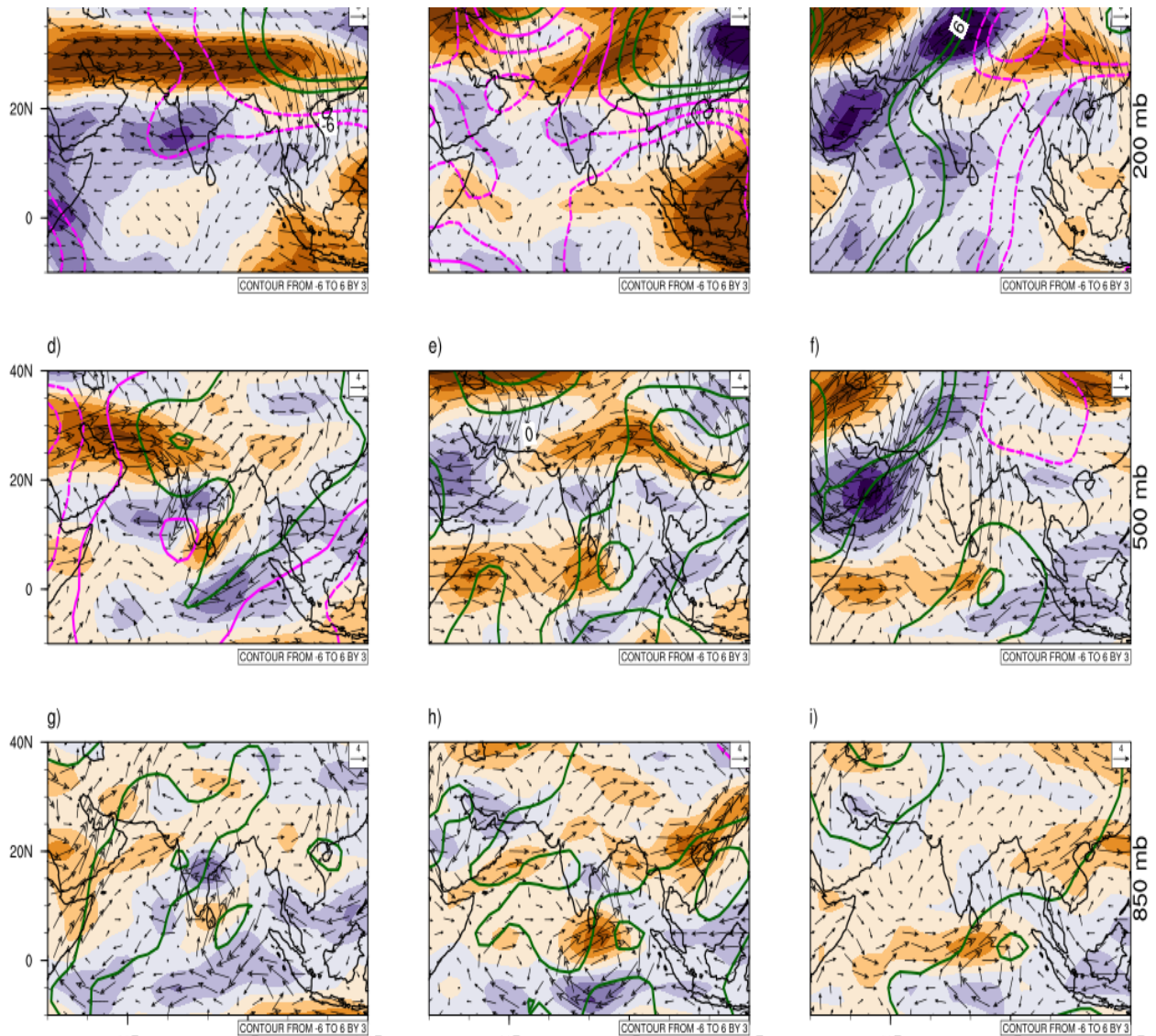
892



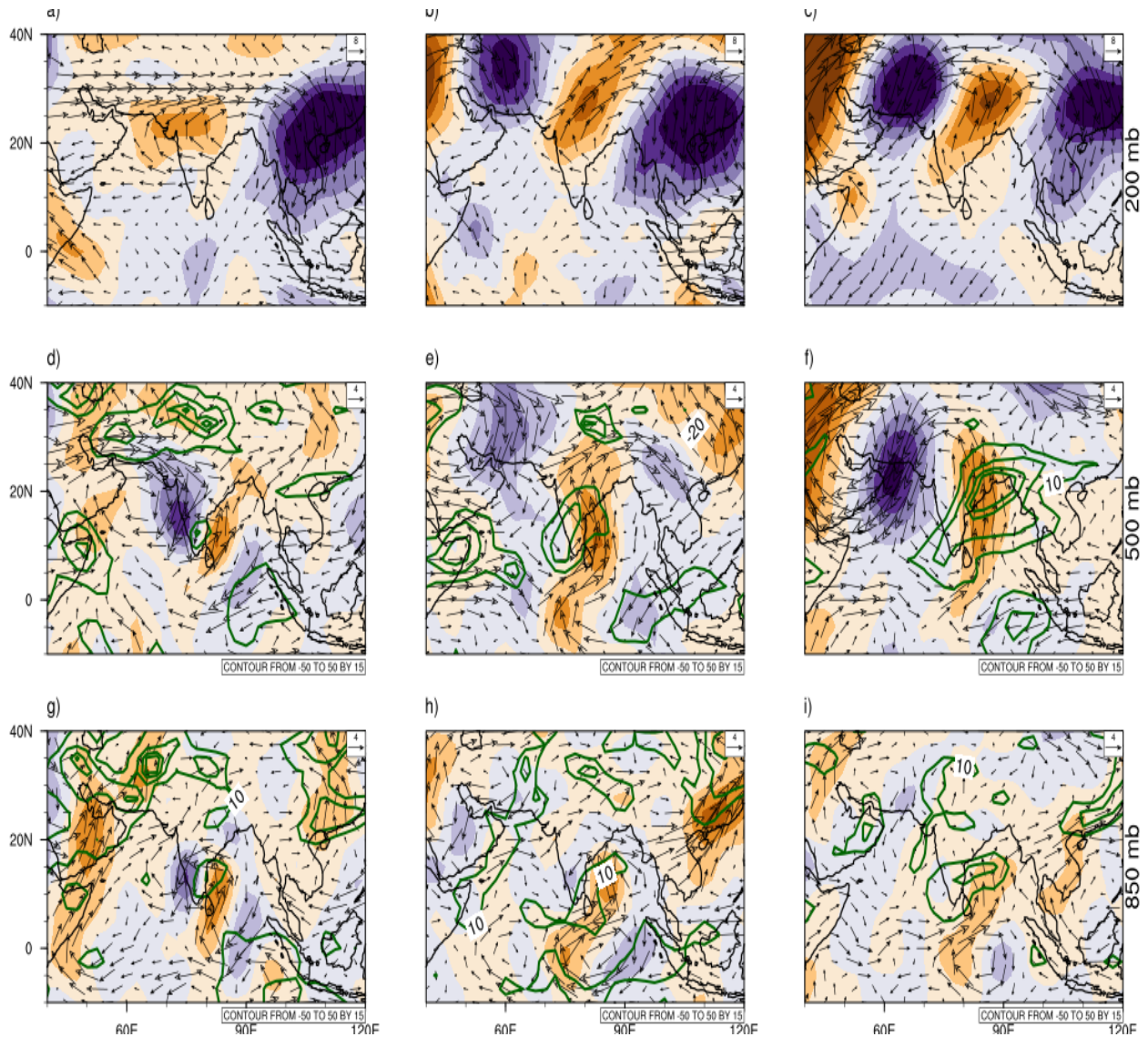
893

894 **Figure 2:** These plots are drawn over latitude 12°N - 13°N and longitude 80°E which covers Chennai
 895 region of India from October 1 to December 31 of 2015. **a)** NCEP precipitation rate (mm/day) averaged
 896 over the mentioned region. **b)** The red color solid line is NCEP lifted index and green color solid line are
 897 NCEP sea level pressure, **c)** NCEP omega anomalies are, **d)** NCEP zonal wind anomalies, and **e)** NCEP
 898 relative humidity anomalies. Note NCEP relative humidity is available up to 300 mb. All of these
 899 variables were composited for case-1 (Nov 9-Nov 10), case-2 (Nov 15- Nov 16), and case-3 (Nov 30-Dec
 900 2), which were mentioned in black color dashed vertical lines.

901



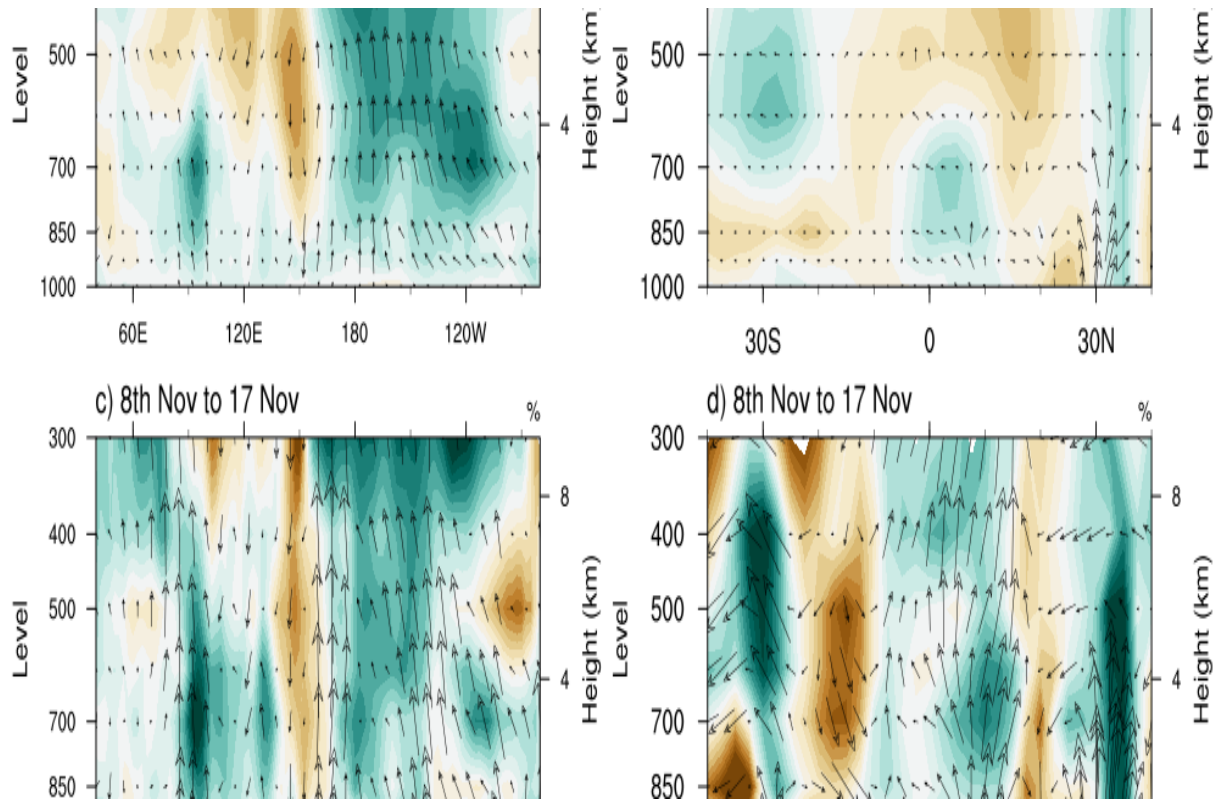
902 **Figure 3:** NCEP zonal wind anomalies composite is created for three cases i.e. (a-d-g) case-1 (Nov 9 to
 903 10), b-e-h) case-2 (Nov 15 to 16), and c-f-i) case-3 (Nov 30-Dec 2). Each row of the panel represents a
 904 pressure level, which is shown to the right of the last column of the panel. A lowermost row of the panel
 905 corresponds to the zonal wind anomalies at 850 mb, and a topmost row of the panel represents 200 mb
 906 zonal wind anomalies. Shaded portion is zonal wind anomalies and vectors are anomalous wind. The
 907 solid contours are positive velocity potential anomalies, and dashed lines are negative velocity potential
 908 anomalies contoured from - 6 to 6 with an interval of three.



909 **Figure 4:** The NCEP meridional wind (m/s) anomalies composite is created for three cases i.e. (a-d-g)
 910 case-1 (Nov 9 to 10), b-e-h) case-2 (Nov 15 to 16), and c-f-i) case-3 (Nov 30-Dec 2). Each row of the
 911 panel represents a pressure level, which is shown to the right of the last column of the panel. A lowermost
 912 row of the panel corresponds to the meridional wind anomalies at 850 mb, and a topmost row of the panel
 913 represents 200 mb meridional wind anomalies. Shaded portion is meridional wind anomalies and vectors
 914 are anomalous wind. The solid contours are positive relative humidity (%) anomalies contoured from -50
 915 to 50 with an interval of 15. Note NCEP Relative Humidity data is available only up to 300 mb pressure
 916 levels.

917

918



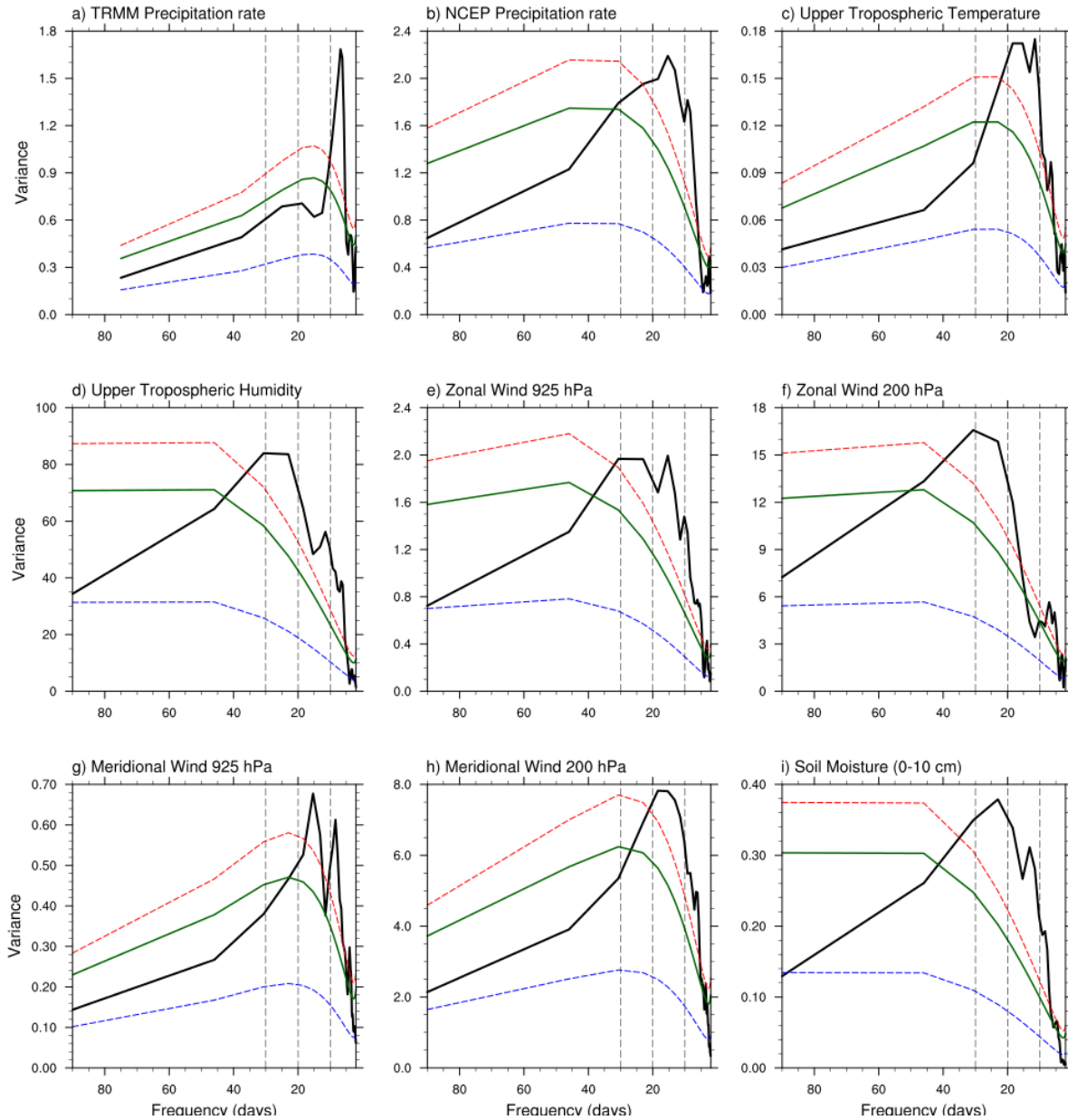
919

920 **Figure 5:** It demonstrates vertical cross-sections of omega, and relative humidity. Left column shows
 921 longitudinal cross-section (a, c) and right column (b, d) represents latitudinal cross-sections. Longitudinal
 922 cross-sections are averaged over 5°S - 5°N , and latitudinal cross-sections are averaged over 75°E - 85°E . Top
 923 row (a, b) represents OND anomalies, and bottom row shows (c, d) mean of the composite from
 924 November 8 to 17, 2015. Here vectors are omega values scaled on the zonal wind for the longitudinal
 925 section and meridional for the latitudinal section.

926

927

928



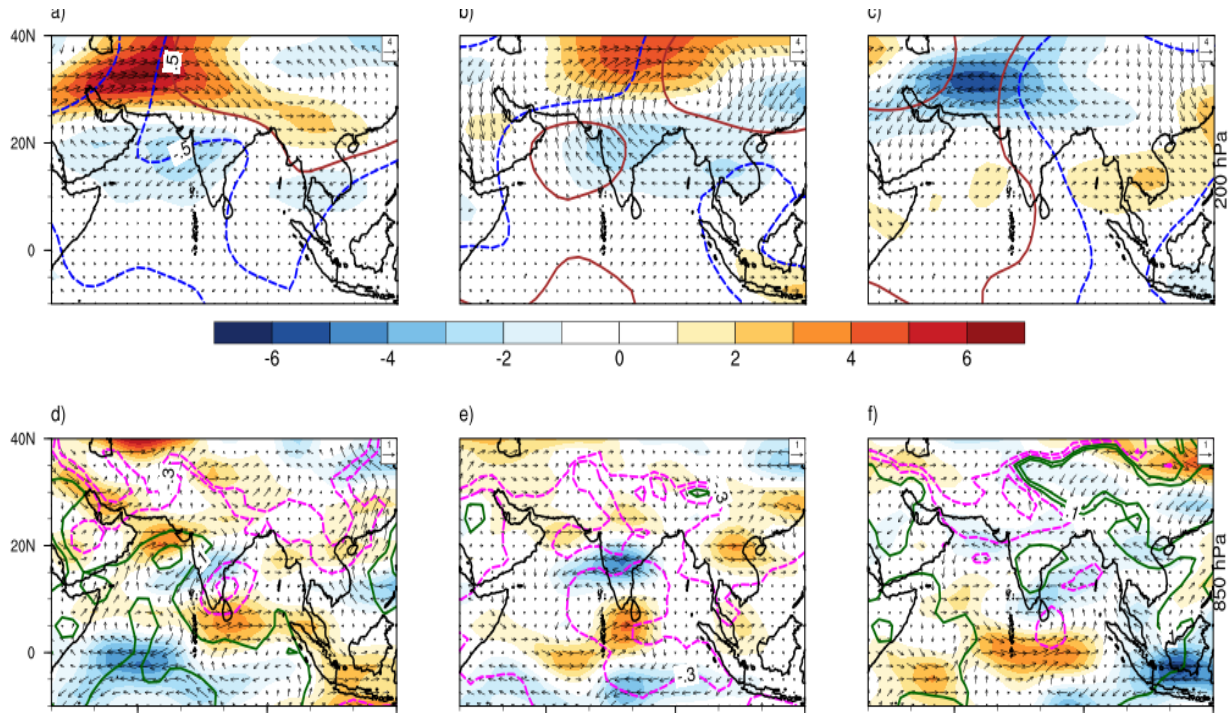
929

930 **Figure 6:** Power spectrum was shown for a) TRMM 3B42 precipitation rate, b) NCEP precipitation rate,
 931 c) air temperature, d) zonal wind at 850 mb, e) soil moisture at 0-10 cm and f) Omega at 850 mb, during
 932 October-December of 2015 over NEM region (8°N-20°N & 70°E-85°E) is calculated. Green Line shows
 933 Markov Red Noise spectrum; red line show upper 95% confidence bounds; and the blue line shows lower
 934 5% limits. The x-axis represents periodicity and y-axis represents variance.

935

936

937



938

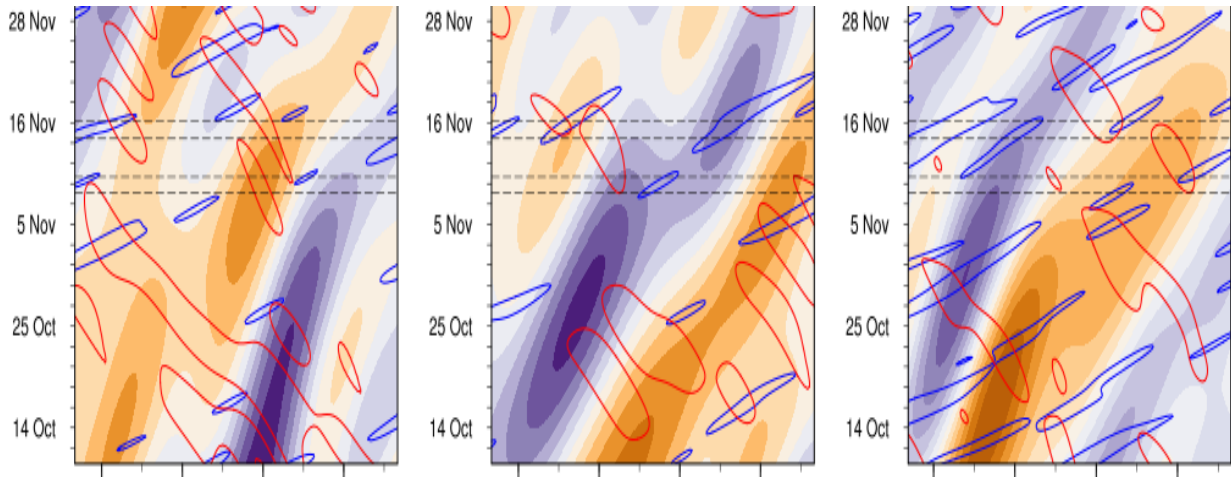
939 **Figure 7:** It displays MJO band pass filtered NCEP zonal wind (m/s) anomalies composite is created for
 940 three cases i.e. (a-d-g) case-1 (Nov 9 to 10), b-e-h) case-2 (Nov 15 to 16), and c-f-i) case-3 (Nov 30-Dec
 941 2). Each row of the panel represents a pressure level, which is shown to the right of the last column of the
 942 panel. A lowermost row of the panel corresponds to the meridional wind anomalies at 850 mb, and a
 943 topmost row of the panel represents 200 mb meridional wind anomalies. Shaded portion and vectors are
 944 band-pass filtered (30-90 days) zonal wind anomalies. In the bottom panel, the dashed contours are
 945 negative sea level pressure (mb) anomalies and solid contours are positive sea level pressure anomalies
 946 contoured for -0.3, -0.1, and 0.3. In the topmost panel, the dashed contour is a negative velocity potential
 947 anomaly, and the solid line is positive velocity potential anomaly contoured for -4.0, -0.5, 0.5, and 4.0.

948

949

950

951



952

953 **Figure 8:** It displays Hovmueller plots of band-pass filtered (30-90 days for MJO, 9-72 days for
 954 equatorial Rossby waves, and 2.5-17 days for Kelvin waves) a) zonal wind anomalies at 850 mb (m/s), b)
 955 zonal wind anomalies at 200 mb (m/s) and c) NCEP precipitation rate (mm/day). They are averaged over
 956 10°S - 10°N . Shaded portion represents MJO filtered waves. Whereas, blue color solid line and red color
 957 solid line represent Kelvin waves and equatorial Rossby waves respectively. Dotted black line points the
 958 dates during which case-1, case-2, and case-3 happened.

959



960 Figure 9: It summarizes the residuals, which are difference between (A) E and N composite (left column), (B) E and M composite, (C) EM
961 blended and N composite, (D) EM blended and M composite, (E) M and N composite, and (F) EM blended and E composite; for NCEP zonal
962 wind anomalies (m/s) and GPCP precipitation rate (mm/day) anomalies. Each row of the panel represents a pressure level, which is shown to the
963 right of the last column of the panel. A lowermost row of the panel corresponds to the wind anomalies at 1000 mb, and precipitation rate
964 anomalies and a topmost row of the panel represents 200 mb zonal wind anomalies. The shaded portions of a second bottom row of the panel to
965 top most rows are zonal wind anomalies. In all of the plots only, more than 95 % significant values are shown (Student's t-test is performed at
966 critical value 0.05).

967



968

969 **Figure 10:** It summarizes the longitudinal vertical cross-sections of omega, and relative humidity
970 anomalies of A, B, C, D, E, and F residuals, which are differences of E & N, E & M, EM & N, EM &
971 M, M & N and EM & E composites, and these composites were explicitly discussed in section 3.6.
972 These longitudinal cross-sections were averaged over 5°S-5°N. Here vectors are omega values scaled w.r.t
973 to the zonal wind, and colored region shows relative humidity anomalies.

974



975

976 **Figure 11:** It describes the latitudinal vertical cross-sections of omega, and relative humidity anomalies of
977 A, B, C, D, E, and F residuals, which are differences of E & N, E & M, EM & N, EM & M, M & N,
978 and EM & E composites, and these composites are apparently discussed in section 3.6. These
979 latitudinal cross-sections were averaged over 75°E-85°E. Here vectors are omega values scaled w.r.t to the
980 meridional wind, and colored area shows relative humidity anomalies.

981

982

983

984

985

986



987

988 **Figure 12:** It demonstrates the response of GPCP precipitation anomalies to NCEP zonal wind anomalies
989 in MJO (red; M), Normal (green; N), El Nino (blue; E) and El Nino & MJO mixed wave (magenta; EM)
990 composites. Here composites are done for a period 1997-2014 in OND season. The black color markers
991 represent the residuals A, B, C, D, E, and F; these residuals are interactions of M & N, E & N, E & M,
992 EM & N, EM & M and EM & E composites respectively. The precipitation anomalies shown above are
993 area averaged over 8°N-16°N & 75°E-84°E, and zonal wind anomalies are area averaged over 0°-6°N &
994 70°E-80°E for MJO and 2°S-4°N & 90°E- 98°E for El Nino composites. The statistical characteristics like
995 p-value (p), correlation coefficient (r), and standard deviations (std) of each composite are also shown in
996 the figure.